

Teemu Myllylä

MULTIMODAL
BIOMEDICAL MEASUREMENT
METHODS TO STUDY
BRAIN FUNCTIONS
SIMULTANEOUSLY WITH
FUNCTIONAL MAGNETIC
RESONANCE IMAGING

UNIVERSITY OF OULU GRADUATE SCHOOL;
UNIVERSITY OF OULU,
FACULTY OF INFORMATION TECHNOLOGY AND ELECTRICAL ENGINEERING,
DEPARTMENT OF ELECTRICAL ENGINEERING



ACTA UNIVERSITATIS OULUENSIS
C Technica 497

TEEMU MYLLYLÄ

**MULTIMODAL
BIOMEDICAL MEASUREMENT
METHODS TO STUDY
BRAIN FUNCTIONS
SIMULTANEOUSLY WITH
FUNCTIONAL MAGNETIC
RESONANCE IMAGING**

Academic dissertation to be presented with the assent of the Doctoral Training Committee of Technology and Natural Sciences of the University of Oulu for public defence in the OP auditorium (L10), Linnanmaa, on 22 August 2014, at 12 noon

UNIVERSITY OF OULU, OULU 2014

Copyright © 2014
Acta Univ. Oul. C 497, 2014

Supervised by
Professor Esko Alasaarela
Professor Anssi Mäkynen

Reviewed by
Professor Frédéric Lesage
Professor Kalju Meigas

Opponent
Professor Raimo Sepponen

ISBN 978-952-62-0506-9 (Paperback)
ISBN 978-952-62-0507-6 (PDF)

ISSN 0355-3213 (Printed)
ISSN 1796-2226 (Online)

Cover Design
Raimo Ahonen

JUVENES PRINT
TAMPERE 2014

Myllylä, Teemu, Multimodal biomedical measurement methods to study brain functions simultaneously with functional magnetic resonance imaging.

University of Oulu Graduate School; University of Oulu, Faculty of Information Technology and Electrical Engineering, Department of Electrical Engineering

Acta Univ. Oul. C 497, 2014

University of Oulu, P.O. Box 8000, FI-90014 University of Oulu, Finland

Abstract

Multimodal measurements are increasingly being employed in the study of human physiology. Brain studies in particular can draw advantage of simultaneous measurements using different modalities to analyse correlations, mechanisms and relationships of physiological signals and their dynamics in relation to brain functions. Moreover, multimodal measurements help to identify components of physiological dynamics generated specifically by the brain.

This thesis summarizes the study, design and development of non-invasive medical instruments that can be utilized in conjunction with magnetic resonance imaging (MRI). A key challenge in the development of measurement methods is posed by the extraordinary requirements that the MRI environment poses - all materials need to be MR-compatible and the selected instruments and devices must not be affected by the strong magnetic field generated by the MRI scanner nor the MRI by the instruments placed within its scanning volume.

The presented methods allow simultaneous continuous measurement of heart rate (HR) and metabolism from the brain cortex as well as pulse wave velocity (PWV) and blood pressure measurements in synchrony with electroencephalography (EEG) and MRI. Furthermore, the thesis explored the reliability and accuracy of the responses gathered by the developed instruments and, using new experimental methods, estimated the propagation of near-infrared light in the human brain.

The goal of the novel multimodal measurement environment is to provide more extensive tools for medical researchers, neurologists in particular, to acquire accurate information on the function of the brain and the human body. Measurements have been performed on more than 70 persons using the presented multimodal setup to study such factors as the correlation between blood oxygen level-dependent (BOLD) data and low-frequency oscillations (LFOs) during the resting state.

Keywords: blood oxygen level, blood pressure, brain, electrocardiography, heart rate, magnetic resonance imaging, multimodal measurements, near-infrared spectroscopy, pulse transit time

Myllylä, Teemu, Multimodaaliset biolääketieteelliset mittausmenetelmät aivojen toimintojen tutkimiseen funktionaalisen magneettikuvauksen yhteydessä.

Oulun yliopiston tutkijakoulu; Oulun yliopisto, Tieto- ja sähkötekniikan tiedekunta, Sähkötekniikan osasto

Acta Univ. Oul. C 497, 2014

Oulun yliopisto, PL 8000, 90014 Oulun yliopisto

Tiivistelmä

Multimodaalisia kuvantamismenetelmiä käytetään enenevässä määrin ihmisen fysiologian ja elintoimintojen tutkimisessa. Erityisesti aivotutkimuksessa samanaikaisesti useammalla modaaliteetilla mittaaminen mahdollistaa erilaisten fysiologisten mekanismien ja niiden korrelaatioiden tutkimisen kehon ja aivotointojen välillä. Lisäksi multimodaaliset mittaukset auttavat yksilöimään fysiologiset komponentit toisistaan ja identifioimaan aivojen tuottamia fysiologisia signaaleja.

Tämä väitöskirja kokoa tutkimustyön sekä laite- ja instrumentointisuunnittelun ja sen kehittämistyön ei-invasiivisesti toteutettujen lääketieteen mittausmenetelmien käyttämiseksi magneettikuvauksen aikana. Erityishaasteena työssä on ollut magneettikuvausympäristö, joka asettaa erityisvaatimuksia mm. mittalaitteissa käytettäville materiaaleille sekä laitteiden häiriönsiedolle magneettikuvauslaitteen aiheuttaman voimakkaan magneettikentän takia. Kehitettävät mittausmenetelmät eivät myöskään saa aiheuttaa häiriöitä magneettikuvauslaitteen tuottamalle kuvainformaatiolle.

Väitöskirjassa esitettävät mittausmenetelmät tekevät mahdolliseksi mitata magneettikuvausympäristössä ihmisen sydämen sykettä, veren virtauksen kulkunopeutta ja verenpaineen vaihteluja sekä aivokuoren metaboliaa - kaikki synkronissa aivosähkökäyrän mittaamisen ja magneettikuvantamisen kanssa. Lisäksi väitöskirjassa tutkitaan kehitettyjen mittausmenetelmien antama mittaustarkkuutta sekä arvioidaan lähi-infrapunavalon etenemistä ihmisen aivoissa uudella menetelmällä.

Kehitetyllä multimodaalisella mittausympäristöllä on tavoitteena antaa lääketieteen alan tutkijoille, erityisesti neurologeille, käyttöön mittausmenetelmiä, joiden avulla voidaan tutkia ihmisen aivojen ja kehon välisiä toimintoja aiempaa kattavammin. Laittekokonaisuudella on tutkittu jo yli 70:tä henkilöä. Näissä mittauksissa on tutkittu mm. veren happitasojen hitaita vaihteluja ihmisen aivojen ollessa lepotilassa, ns. resting state -tilassa.

Asiasanat: aivot, lähi-infrapunaskpektroskopia, magneettikuvaus, multimodaaliset mittausmenetelmät, pulssinkulku-aika, sydämensyke, sydänsähkökäyrä, veren happitaso, verenpaine

To Pietari, Auri and Anna

Preface

Brain functions have fascinated us humans through the ages, particularly those of us who practice medicine. In terms of brain imaging, the achievements of modern medical science are admirable, and it is now, for example, possible to visualize the brain structure and to study connections between neurons. However, metabolism and blood flow-related dynamics in the brain are still relatively little examined, which is why they are now attracting the attention of developers of new measurement methods.

The Optoelectronics and Measurement Techniques Laboratory (OEM) has been designing and developing measurement methods for medical research and practice already many decades. One area of specific interest has been blood and cardiovascular related measurements. However, developing medical measurements for the study of the brain is still a new field for our laboratory, and this thesis is the first doctoral study focussing on it. The first magnetic resonance imaging (MRI)-related project at our lab, “Surgical, Interactive Robot Developed into MRI”, was launched in 2005. I was lucky to get involved in this project, mainly thanks to my knowledge of EMC, acquired from previous projects. I got the opportunity to conduct MRI-compatibility test measurements inside an MRI room with the help of a hospital physicist, Jani Katisko, PhD. My responsibility was to develop MRI-compatible data transfer and camera techniques for the robot, while mainly Hannu Sorvoja, DSc and Juha Harja, Tech.Lic, from our laboratory, were focusing on controlling the movements of the robot arm. Successful completion of the project gave us a head start for developing MRI-compatible instrumentation in general.

In 2007, Docent Vesa Kiviniemi, specializing in neuroradiology, contacted our laboratory, because he was eager to broaden the range of methods used to study the brain. This launched our laboratory into the study of biomedical measurement methods for the brain. The first project was entitled “Multimodal Evaluation of Brain Oscillations” and it ran from 2008 to 2011. Right away, basically from scratch, we started developing methods to measure blood pressure and blood oxygen levels in the brain during MRI. From our laboratory, Juha, Hannu and I were most involved in this undertaking, because we already had a good knowledge of the MRI environment and medical instrumentation. Unfortunately, a couple of years later, Juha decided to move on, leaving just Hannu and me working on the project. Soon afterwards, Vesa Korhonen joined our laboratory to work on his Master’s thesis, which was related to our project,

while Hannu started focussing more on other duties at the lab by the end of the project. For the past few years, I have been developing the multimodal measurement methods and setup presented in this thesis, mainly in collaboration with Vesa Korhonen, and together with the Oulu Functional NeuroImaging group, led by Vesa Kiviniemi, we have conducted medical measurements using the system. To further develop it, we joined forces with the Biophotonics group of our lab, supported by Professor Valery Tuchin with financing provided by the Finland Distinguished Professor (FiDiPro) programme, and carried out a series of test measurements with optical phantoms.

In addition to regular working time, Vesa Korhonen and I have spent many weekends and evenings in our free time developing and testing devices and analysis methods. We have carried the heavy equipment at least 100 times from the university campus to the university hospital and back. I'm lucky to have Vesa as a colleague - we have a joint interest in the system and have not counted the hours required to make it. In my view, we have succeeded in building a unique multi-modal measurement system with a great potential for the study of the brain. Credit for the completion of the system goes to all persons involved and to the creative co-operation fostered between the OEM laboratory and the Department of Diagnostic Radiology.

Acknowledgements

I wish to express my deepest gratitude to Docent Vesa Kiviniemi, MD, PhD and emphasize his impact on my doctoral studies. He has enabled the development of the multimodal setup and has given me the possibility to take part in several interesting brain-related medical studies. His open-minded and enthusiastic way of approaching medical research has inspired me and many others.

I would like to thank my first supervisor, Professor Esko Alasaarela, and second supervisor, Professor Anssi Mäkynen, for supervising my thesis. I appreciate your encouragement and feedback, as well as the freedom to independently determine the focus of my research.

I am very grateful for having had the opportunity to closely co-operate with the Oulu Hospital and Medical Research Center, particularly with the departments of Diagnostic Radiology, Neurology, Anaesthesiology and Oncology. Special thanks for support and co-operation go to doctors of medicine Professor Osmo Tervonen, Professor Outi Kuittinen, Eila Sonkajärvi, PhD Hanna Ansakorpi, PhD, medical physicists Juha Nikkinen, PhD, Jani Katisko, PhD and PhD students Vesa Korhonen and Tuija Hiltunen as well Elina Kansanoja.

Moreover, I wish to extend my warmest thanks to Martin Walter, MD, PhD, and his colleagues for the opportunity to carry out medical measurements with the multimodal setup at the Leibniz Institute for Neurobiology in Magdeburg.

I am grateful to the Department of Metrology and Optoelectronics, Gdansk, for fruitful co-operation. I am particularly indebted to Professor Jerzy Pluciński, Małgorzata Jedrzejewska-Szczerska, PhD, Aleksandra Zienkiewicz, MSc, Łukasz Suraczyński, MSc, and many others who have visited our laboratory in the past few years. I have very keen memories of Professor Henryk Wierzba (deceased), who encouraged me in the early stages of my studies.

I'm very thankful for having the opportunity to work in the Optoelectronics and Measurement Techniques Laboratory, and I'd like to thank the entire personnel for creating a good working atmosphere. I am especially thankful for the close co-operation offered by Hannu Sorvoja, DSc, who has played an important role in my professional career, particularly at the start of my research work. I give my warmest thank for the co-operation to Juha Harja, Tech.Lic, with whom I worked in the beginning of this project, and Erkki Vihriälä, MSc. From the Biophotonics group, Matti Kinnunen, DSc, Alexey Popov, DSc, Alexander Bykov, DSc, and Zuomin Zhao, DSc all receive my warmest expression of gratitude. My sincere gratitude must also be extended to the many internship

students that I have had the opportunity to supervise and work with, especially MSc student Marco Perez Leandro from Spain. Thanks are also due to Kari Remes, MSc, and his predecessor, Jorma Honkala, Tech.Lic, who sadly passed away last year, for their support in laboratory techniques.

Special thanks go to our FiDiPro-Professor Valery Tuchin for his support. His high scientific level I can only admire.

I deeply acknowledge the efforts of all 18 co-authors from many different countries. Without your co-operation my thesis would never have got off the ground!

I wish to express my sincere thanks to the pre-examiners Professor Kalju Meigas from Tallinn University of Technology and Professor Frédéric Lesage from Polytechnique Montréal for reviewing this thesis. I greatly appreciated all your comments. Also, I warmly thank Professor Raimo Sepponen from Aalto University for acting as opponent for this thesis.

I gratefully acknowledge the financial support provided by the following foundations: Seppo Säynäjäkankaan Tiedesäätiö (two grants) and Tauno Tönnöngin Säätiö. I am also thankful for the travel grant received from the Oulu Graduate School.

Many thanks to Rauno Varonen, Phil.Lic, for fast, but accurate language checking of my thesis.

Last but not least, I thank my family. Especially, I'd like to thank Mari for her long-time support. Thanks to my grandmother Betty for being such a lovely person. Most of all, I'd like to thank my father. It has been a pleasure to communicate with him also in work-related situations.

Oulu, June 2014

Teemu Myllylä

List of terms, symbols and abbreviations

ACR	American College of Radiology
AM	Amplitude Modulation
AMP	Amplifier
aMEG	anatomically-constrained magnetoencephalography
BBB	Blood-Brain Barrier
BBBD	Blood-Brain Barrier Disruption
BLL	Beer-Lambert Law
BOLD	Blood Oxygen Level Dependent
BP	Blood Pressure
CBF	Cerebral Blood Flow
CBV	Cerebral Blood Volume
CO ₂	Carbon Dioxide
CTA	Computed Tomography Angiography
CW	Continuous Wave
DAQ	Data Acquisition
DOI	Diffuse Optical Imaging
DOS	Diffuse Optical Spectroscopy
DOT	Diffuse Optical Tomography
DPF	Differential Path-length Factor
ECG	Electrocardiography
EEG	Electroencephalography
EMC	Electromagnetic Compatibility
EMI	Electromagnetic Interference
exNIR	Extended Near-Infrared
expCO ₂	Expired Carbon Dioxide
FD	Frequency Domain
FiDiPro	Finland Distinguished Professor Programme
fMRI	Functional Magnetic Resonance Imaging
fNIRS	Functional Near-infrared Spectroscopy
HbO ₂	Oxyhaemoglobin
HbO	Oxyhaemoglobin
Hb	Haemoglobin, Deoxyhaemoglobin
HbR	Reduced Haemoglobin, Deoxyhaemoglobin
HbT	Total Haemoglobin
HCI	Host Controller Interface

HEC	Header Error Control
HPLED	High Power Light Emitting Diode
HR	Heart Rate
IBP	Invasive Blood Pressure
iMRI	Intraoperative Magnetic Resonance Imaging
ISM	Industrial Scientific and Medical Band
LASER	Light Amplification by Stimulated Emission of Radiation
LD	Laser Diode
LED	Light Emitting Diode
LFO	Low-Frequency Oscillation
LOA	Limit Of Agreement
LP	Low Pass
MBLL	Modified Beer-Lambert Law
MC	Monte Carlo
MEG	Magnetoencephalography
MRI	Magnetic Resonance Imaging
MREG	Magnetic Resonance Encephalography
NIBP	Non-Invasive Blood Pressure
NIR	Near-infrared
NIRI	Near-infrared Imaging
NIRS	Near-infrared Spectroscopy
OD	Optical Density
OEF	Oxygen Extraction Fraction
OEM	Optoelectronics and Measurement Techniques Laboratory
OFNI	Oulu Functional NeuroImaging
OPL	Optical Path Length
PET	Positron Emission Tomography
PM	Phase Modulation
PPG	Photoplethysmography
PS	Phase Shift
PSD	Phase Sensitive Detector
PTT	Pulse Transit Time
PWV	Pulse Wave Velocity
QRS complex	Depolarization of the ventricles
RFID	Radio-Frequency Identification
SNR	Signal-to-Noise Ratio
SPO ₂	Saturation of Peripheral Oxygen

SpO ₂	Pulse Oximeter Oxygen Saturation
SRD	Short Range Devices
SRS	Spatially Resolved Spectroscopy
TD	Time Domain
USB	Universal Serial Bus
VMW	Vasomotor Wave
WLAN	Wireless Local Area Network

List of original papers

This thesis is based on the following publications and their respective studies:

- I Myllylä T, Katisko J, Harja J, Sorvoja H & Myllylä R (2007) EMI considerations for wireless data transfer in magnetic resonance imaging (MRI) operating room. The 2nd International Symposium on Medical Information and Communication Technology (ISMICT 07), 11-13 December 2007, Oulu, Finland. Proceedings: 1–4.
- II Sorvoja H, Myllylä T, Kirillin MYu, Sergeeva E, Myllylä R, Elseoud AA, Nikkinen J, Tervonen O & Kiviniemi V (2010) Non-invasive, MRI-compatible fibre optic device for functional near-IR reflectometry of human brain. *Quantum electronics* 40: 1067–1073.
- III Myllylä T, Elseoud AA, Sorvoja H, Myllylä R, Harja J, Nikkinen J, Tervonen O & Kiviniemi V (2011) Fibre optic sensor for non-invasive monitoring of blood pressure during MRI scanning. *J. Biophoton* 4 (1–2): 98–107.
- IV Myllylä T, Korhonen V, Vihriälä E, Sorvoja H, Hiltunen T, Tervonen O & Kiviniemi V (2012) Human heart pulse wave responses measured simultaneously at several sensor placements by two MR-compatible fibre optic methods. *Journal of Sensors*, vol. 2012, Article ID 769613: 1–8.
- V Myllylä T, Vihriälä E, Korhonen V & Sorvoja H (2013) Case study of ECG signal used as a reference signal in optical pulse transit time measurement of blood flow – The effect of different electrode placements on pulse transit time. *Proc. of SPIE Vol. 8699*: 869903–1–13.
- VI Toronov V, Myllylä T, Kiviniemi V & Tuchin VV (2013) Dynamics of the brain: mathematical models and non-invasive experimental studies. *The European Physical Journal Special Topics* 222(10): 2607–2622.
- VII Myllylä T, Popov A, Korhonen A, Bykov AV & Kinnunen M (2013) Optical sensing of a pulsating liquid in a brain-mimicking phantom. *Proc. of OSA-SPIE* 8799: 87990X–1–7.

These papers are referred to in the text by Roman numerals (I–VII). The current author is either the first or second author in all these publications.

Paper I studies requirements imposed by magnetic resonance compatibility and electromagnetic interference (EMI) on the magnetic resonance imaging (MRI) environment. It also presents measurements of EMI generated by an MRI scanner, together with test results of wireless data transfer using five different techniques within an MRI room during MRI scanning.

Paper II introduces an MRI-compatible device for non-invasive measurements of blood oxygen variations in the brain cortex. It then describes the design and functioning of a fibre optic device based on near-infrared spectroscopy

(NIRS). The Monte Carlo calculation of light attenuation shown in the paper was performed by Mikhail Kirillin and Ekaterina Sergeeva.

Paper III introduces a novel fibre optic measurement method for non-invasive monitoring of blood pressure (BP) during MRI scanning. The used acceleration sensor was originally designed by Juha Harja and Hannu Sorvoja. Additionally, the paper describes a method of using pulse wave velocity (PWV) to estimate diastolic BP.

Paper IV shows that the propagation of pressure waves generated by each heart pulse can be sensed extensively in different areas of the human body during MRI. Experimental measurements, involving several test patients, were performed both inside and outside an MRI room. Accuracy of the gathered heart pulse wave responses and their pulse shapes for estimating pulse transit time (PTT) is discussed.

In paper V, the shape of the QRS complex (the complex consisting of Q, R, and S waves, corresponding to depolarization of ventricles), particularly the position of R wave in the QRS complex, is studied using different electrocardiography (ECG) electrode placements. This study is related to calculation of the PTT between R waves of the ECG signal and BP pulsation signals measured by photoplethysmographic (PPG) sensors.

Paper VI reviews experimental non-invasive techniques developed to study brain functions and to measure dynamic characteristics, such as neurodynamics, neurovascular coupling, haemodynamic changes due to brain activity and autoregulation as well as the cerebral metabolic rate of oxygen. It also shows experimental studies and results obtained by the designed measurement methods, described in the previous papers. A major part of the fMRI correlation analysis provided in the paper was conducted by Vesa Kiviniemi with the help of Vesa Korhonen and Jaakko Vanhatalo.

Paper VII studies light propagation within brain tissue and introduces an experimental method to estimate the depth of light penetration into the brain. Based on the presented measurements, the paper concludes that pulsations from a grey matter mimicking layer of the brain can be detected at a source-detector distance of 3 - 4 cm, using the measurement technique described in papers II and IV. The fabrication process of the optical phantoms, used in this study, was originally developed by Alexander Bykov and Alexey Popov.

Contents

Abstract	
Tiivistelmä	
Preface	9
Acknowledgements	11
List of terms, symbols and abbreviations	13
List of original papers	17
Contents	19
1 Introduction	21
1.1 Focus and scope of the thesis	21
1.2 Background of the utilised measurement methods.....	21
1.2.1 Optical methods for the study of the brain	24
1.3 Motivation.....	26
1.4 Objectives, contribution and novelty of the thesis	28
1.5 Outline of the thesis	29
2 MRI room as a measurement environment	31
2.1 Electromagnetic interference (EMI) and MRI compatibility	31
2.2 Placement of the instruments and devices.....	32
2.3 Data transfer inside the MRI room.....	34
3 Methods of measurement and the multimodal setup	39
3.1 Optical NIRS-based measurement method to monitor metabolism and blood flow pulsations during MRI.....	39
3.1.1 Utilization of high power LEDs in illumination.....	40
3.1.2 Lock-in amplification for detecting and separating different wavelengths	42
3.1.3 Quantifying tissue metabolism on the basis of received signals.....	47
3.2 Continuous measurement of BP pulsations during MRI.....	51
3.2.1 Estimation of continuous BP based on pulse wave velocity.....	54
3.3 Realization of the multimodal measurement setup	56
4 Results to validate the methods	61
4.1 MRI compatibility of the measurement methods.....	61
4.2 Sensing by the NIRS device.....	63
4.3 HR and BP pulsation measurements	67
4.4 Synchronised response of different pulsations during MRI.....	73

5 Discussion	77
5.1 Limitations and possible improvements.....	77
5.1.1 Spatial resolution of NIRS.....	77
5.1.2 R peak of the QRS complex to calculate PTT during MRI	79
5.1.3 NIBP by accelerometers	79
5.1.4 Technical improvements of the NIRS device	80
5.1.5 Development of a wearable NIRS sensor	80
5.2 Current and future work with the multimodal setup	81
6 Conclusion	83
References	85
Original papers	93

1 Introduction

1.1 Focus and scope of the thesis

At the core of this thesis sit non-invasive measurements of human physiology, particularly HR, blood flow and pressure in blood and tissue. All of these physiological dynamics are simultaneously present in the human body. By monitoring the physiological dynamics from different parts of the body, we may study the functioning of organs and gain a better understanding of the interconnections between different physiological activities. Of particular interest here is brain activity. For this purpose, the goal was to develop a multimodal measurement environment for magnetic resonance imaging (MRI). This type of environment would widen our current range of methods for measuring physiological dynamics during MRI to allow a more comprehensive study of the brain. A multimodal system extends our options to acquire detailed knowledge of such topics as how the brain interrelates with other organs and how blood flows in the human body. Other uses include helping to identify normal and abnormal functioning of the brain caused by brain-related diseases, such as epilepsy and narcolepsy. This thesis, however, focuses on developing measurement methods for brain studies and on estimating the reliability of the gathered data. Due to the engineering educational background of the author, the thesis does not concern itself with medical data analysis, although the presented system is already being used in several medical studies involving the author as participant.

1.2 Background of the utilised measurement methods

Throughout the history of health science, cardiac and vascular function has been an important indicator for estimating a person's health condition. Nowadays, the evaluation process is commonly based on non-invasive ECG and BP measurements. Both these methods have been in clinical use for decades and a detailed understanding of differences between normal and abnormal functions has been developed. This knowledge is now being utilized also in preventive medicine. Both ECG and BP measurements have a long history. The first published measurement of BP was done in 1733 by Stephen Hales (Smith 1993). Cuff-based BP measurements were introduced by Scipione Riva-Rocci in 1896 and were in common use in the first half of the 20th century. In recent decades,

various methods have been developed to estimate BP non-invasively (Hakim 2011). As most of them rely on using a cuff, they can provide highly accurate absolute blood pressure values, though not continuously as a function of time. Continuous NIBP measurements are mostly based on an analysis of pulse shape or pulse transit time (PPT) of blood flow, sometimes also including using a cuff (Gribbin *et al.* 1976; Kerola *et al.* 1996; Hast 2003; Meigas *et al.* 2004; Lass *et al.* 2004; Sorvoja 2006; Sugo *et al.* 2012). The accuracy of existing non-invasive methods has improved continuously, and the current clinically acceptable limit of agreement (LOA), +15 mm Hg, set by the American Association for the Advancement of Medical Instrumentation for NIBP measurements, has already been achieved with several NIBP measurement methods (Gesche *et al.* 2012; Hahn *et al.* 2012). Nevertheless, accurate continuous absolute blood pressure values can only be reliably obtained by invasive methods. Moreover, a comprehensive comparison of NIBP with invasive BP is difficult, particularly because invasive method tends to require that the subject to be measured stays still, because invasive methods are difficult to perform on a moving person.

The invention of ECG is credited to William Einthoven in the year of 1895 (Moukabary 2007), although the first instruments for sensing the small electrical currents flowing in the heart were designed as early as in the first half of the 19th century. The first portable ECG was built by a medical equipment manufacturer in 1928, but more common clinical investigations involving ECG started after the Second World War (Jenkins & Gerred 2009). Today, ECG and BP methods are portable and BP measurements in particular can be performed at home. Development of these devices formed a basis to and facilitated the development of modern medical instrumentation and biomedical imaging.

Generally, it may be said that the modern study of brain functions began with the discovery of electrical activity in the brain, right after the invention of ECG. However, it is worth mentioning that the very first studies of the brain were conducted by Angelo Mosso in the 1880s, when he invented the so-called “human circulation balance”, to non-invasively measure the redistribution of blood during emotional and intellectual activity (Sandrone *et al.* 2014). Nevertheless, initial studies of brain function were mainly based on measuring electrical activity from the human head by means of electroencephalography (EEG). These measurements started in the year of 1924, when Hans Berger used an electrode to record electrical activity on the scalp (Berger 1929). Later on, development of the EEG led to the use of topographic scalp maps, which record activity of underlying brain structures by electrodes placed at certain points on the

head. Commonly, studies based on recording electrical activity of the brain still rely on the same method. In EEG measurements, scalp electric potential differences are determined by electric neuronal activity from the entire cortex and by the geometrical orientation of the cortex. This makes it hard to accurately determine the actual generators of current on the basis of scalp electric potentials. Furthermore, it is mathematically impossible to reconstruct current sources for a given EEG signal, as some currents produce potentials that cancel each other out. This is referred to as the inverse problem (Tong *et al.* 2009). EEG has a high temporal resolution, on the millisecond scale, which is adequate to follow brain activity changes. On the other hand, the method has a relatively modest spatial resolution, on the centimetre scale. This is a notable weakness of EEG, since brain studies place particular importance on precise localization of brain functions.

More advanced neuroimaging of the brain became a reality in the 1960s and 1970s. In addition to the development of computerised tomography and radioactive neuroimaging, the invention of magnetic resonance imaging (MRI) in 1977 by Raymond Damadian had a major impact on the field. During the 1980s, technical improvements and new diagnostic methods led to the discovery that oxygen in liquid state is influenced by the presence of a magnetic field. It was realized that blood, which contains oxygen, is also indirectly influenced by magnetic fields. This allowed the application of MRI to the study of brain activity based on observing blood oxygen changes in different parts of the brain (Ogawa *et al.* 1990 & 1992, Biswal *et al.* 1995, Dyer 2006). Since the 1990s, functional magnetic resonance imaging (fMRI) has come to dominate brain mapping due to lack of radiation exposure and availability. However, it still suffers from rather poor time resolution, approximately from 1 to 2 Hz. In recent years, though, major improvements in time resolution have been reached by new scanning techniques, such as magnetic resonance encephalography (MREG), which at the moment can reach a time resolution of 10 to 16 Hz (Hugger *et al.* 2011, Assländer *et al.* 2013).

It is also common practice to compensate for the low time resolution of MRI by using other measurement methods with a higher time resolution. This leads to setting up multimodal imaging systems, where the basic idea is to combine the best features of various measurement methods and modalities. One of the newest techniques utilizing multimodal methods in brain studies is anatomically-constrained magnetoencephalography (aMEG) (Marinkovic *et al.* 2011). This

method combines the high spatial resolution of MRI with the high temporal resolution of MEG.

The brain is strongly dependent on cardiac and vascular function. As a matter of fact, 20% of the blood is delivered to the brain (Carvey *et al.* 2009). For example, if the brain is without blood for more than one second, damage may occur. By knowing this, it is easy to understand how essential blood flow is for the brain. Blood delivers not only oxygen to the brain, but also other vital substances, such as glucose, which is used for energy. During the recent decades, while we have started to better understand the functioning of the cardiac and vascular system, a growing interest has been paid to studying the relationships between this system and brain function. This work has also resulted in a need to develop multimodal measurement methods. Fortunately, corresponding achievements in the field of biophotonics have produced optical methods that lend themselves to the study of the brain, especially brain metabolism (Tuchin 2002).

1.2.1 Optical methods for the study of the brain

Diffuse optical spectroscopy (DOS) is a method for quantifying the biochemical state of a substance or tissue on the basis of its absorption and scattering properties. Conducted by Jöbsis in 1977, the first DOS-based brain studies managed to measure oxygenation changes in the brain of an animal (Jöbsis 1977). Since then, an increasing number of clinical and research applications related to DOS have seen the light of day.

DOS is often referred to as near-infrared spectroscopy (NIRS), functional NIRS (fNIRS), near-infrared imaging (NIRI), diffuse optical imaging (DOI) or diffuse optical tomography (DOT). Among these, perhaps the most commonly used acronym is NIRS, but DOS, DOI and DOT, standing for different methods used in the field, can be used to put specific emphasis on spectroscopy, imaging or tomography (Madsen 2013). The author prefers to use the more general term, NIRS, also when referring to the device developed in the course of this work (II).

In measurements of the cerebral cortex, NIRS has many advantages over other neuroimaging methods, such as fMRI or positron emission tomography (PET) (Misciagna 2013). NIRS is much more cost-effective and does not require a special measurement environment. Most importantly, it offers a broad range of contrast mechanisms for the study of blood flow-related metabolism (Cooper 1997, Obrig 2014). One particular advantage is the ability to simultaneously

measure blood volume (HbT) and both oxyhaemoglobin (HbO₂ or HbO) and deoxyhaemoglobin (Hb or HbR) at a high time resolution. As for fMRI, it typically exploits the blood oxygen level dependent (BOLD) signal, which is widely thought to correlate with Hb. However, a BOLD increase (an Hb decrease) may correspond to an increase in oxygenation, or a decrease in blood volume (Hillman 2007). The biggest disadvantage of NIRS is its low spatial resolution and scanning depth. Depending on the sensor arrangement and obtained measurement depth, its spatial resolution is in the range of 1 to 2 cm, and the scanning depth in the brain is commonly less than 3 cm.

Near-infrared (NIR) spectrometers typically use three techniques, related to a specific technique of illuminating the brain (Ferrari *et al.* 2012). First, there is the continuous-wave (CW) technique, in which the illuminating light has a constant frequency and amplitude and only light attenuation is measured. (Kurth *et al.* 1999, Zoe *et al.* 2010). Secondly, the time-domain (TD) technique uses a very short illuminating NIR pulse, generally with a pulse length of a few picoseconds, while the photon path-length is based on time-of-flight (Delpy & Cope 1997; Re *et al.* 2013). Finally, the frequency-domain (FD) method is based on modulating the intensity of the illuminating light and measuring both the attenuation and phase delay of the emerging light. Because phase measurements and intensity modulation are the key features of FD spectroscopy, the term phase-modulation (PM) is sometimes also used in conjunction with FD. Theoretically, approaches TD and FD avoid the need for actual photon path length determination, because tissue absorption coefficients can be measured directly based on multi wavelength NIRS (Murkin *et al.* 2009). Different NIR spectrometers and their key features and parameters have been reviewed in detail, for example, in the following publications (Ferrari *et al.* 2004; Wolf *et al.* 2007) and handbooks (Tuchin 2002; Madsen 2013).

Illuminating light in a NIRS system typically covers the wavelength range of 600nm to 1000nm, where overall absorption is sufficiently low, allowing light penetration into brain tissue. This wavelength range is sometimes referred to as optical window. In brain tissue, penetration depth can be increased by using the extended near-infrared range (exNIR), a spectral region ranging from 900 to 1400 nm, but lack of suitable detectors has been limiting the utilization of this range, known as the second optical window. Due to improvements in detector technology, this range is attracting a growing interest (Qian *et al.* 2013, Cao *et al.* 2013, Ishikawa *et al.* 2014). Spectral range from 600 nm to 1600 nm is also known as the therapeutic or diagnostic window (Tuchin 2007).

Several commercial NIRS systems as well as non-commercial prototypes are available for brain monitoring (Wolf *et al.* 2007). fNIRS-based studies of the brain are commonly conducted outside the MRI room, due to MR-compatibility requirements. The first simultaneous combined fMRI and fNIRS measurement was carried out in 1996 by a group from the Humboldt University of Berlin in collaboration with Frahm (Max Planck Institute for Biophysical Chemistry, Göttingen, Germany) to measure cerebral blood oxygenation changes during human brain activation (Kleinschmidt *et al.* 1996; Ferrari *et al.* 2012). Although this combined measurement method is still new and not frequently used, largely owing to MRI-compatibility requirements, some publications discuss simultaneous fMRI and fNIRS studies, mostly to validate the correlation between the BOLD signal and cortical hemodynamic changes (Toronov *et al.* 2001; Strangman *et al.* 2002; Hoge *et al.* 2005; Hubbert *et al.* 2006; Steinbrink *et al.* 2006; Cui *et al.* 2011; Duan *et al.* 2011; Tong *et al.* 2010 - 2013; VI). Very recently, a group at Norris Cotton Cancer Center at Dartmouth-Hitchcock has started developing a combined system for diagnostic breast cancer imaging. Moreover, a simultaneous quantitative assessment of cerebral physiology using respiratory-calibrated MRI and near-infrared spectroscopy in healthy adults has been published by (Alderliesten *et al.* 2014). An experimental combined NIR/MRI system has been applied also to animal studies, for instance to rat brain imaging (Xu *et al.* 2005)

Naturally, outside MRI, NIRS-based techniques have been used already in numerous studies, very recently for instance in case studies of sleep (Virtanen 2011, Zhang *et al.* 2013), investigation of verbal and visual working memory (Contini *et al.* 2013), monitoring the oxygen saturation of cerebral tissue during surgery (Meng *et al.* 2013) as well as in study of Alzheimer's disease (Chou *et al.* 2013) and aging of the brain (Lesage *et al.* 2013).

1.3 Motivation

Currently, there is a strong trend in neuroimaging to utilize simultaneous multimodal measurements, such as combined EEG and fMRI or EEG and fNIRS (Näsi *et al.* 2010) measurements. The concept seems to be that a comprehensive understanding of the brain and its functioning requires a simultaneous exploration of the brain and other physiological signal sources, such as blood pressure, during brain activity. This can only be achieved by multimodal measurements, which provide extensive knowledge of the dynamics of the whole body and enable an

analysis of the correlations, mechanisms and relationships of physiological signals and their dynamics in relation to brain function. Combining data from different techniques allows a description of human brain activity using a range of spatial and temporal precision and contrast mechanisms that is impossible to achieve by any single imaging modality (Ferrari *et al.* 2012). Combined fMRI and fNIRS, in particular, may provide a novel contrast mechanism that can be exploited as a tool for a direct characterization of cerebral blood flow (CBF). Moreover, optimization of the technique may allow quantifying other blood flow parameters (Tong *et al.* 2010), for instance, the oxygen extraction fraction (OEF) and cerebral blood volume (CBV) (Toyoda *et al.* 2007; Bakker *et al.* 2012). Human physiological signals also affect each other. For example, HR is affected by normal breathing due to coupling and interaction between the cardiac and respiratory systems (Indic *et al.* 2008). Absence of multimodal measurements severely limits our possibilities of analyzing these interactions. Additionally, multimodal measurements help to identify components generated specifically by the brain, which is important, because dynamics from other organs impact signals measured from the brain. Recent studies based on using multimodal methods have discovered, for instance, that a relationship seems to exist between vasomotor blood pressure fluctuations and brain signals (Kiviniemi *et al.* 2008). One of the challenges particular to this kind of study involves measuring and separating vasomotor wave (VMW) signals that are physiologically related to neural activity fluctuations. This requires isolating other pressure signals, such as signals coming from large arteries and veins and is possible only by utilizing multimodal measurements.

As already stated, one major obstacle for a wider usage of NIRS is its limited depth penetration. Moreover, it fails to provide accurate spatial information. At the moment, Monte Carlo (MC) simulations are the gold standard for simulations of diffuse optical sensing in the brain. However, due to the complex structure of the human head, it is impossible to theoretically describe light propagation and accurately evaluate the measurement volume of a NIRS setup (Korhonen *et al.* 2014). This is the case especially when the separation distance between the source and detector of the NIRS sensor is long, as illuminating light propagates to a wider area inside the tissue before reaching the detector. Therefore, another motivation for this thesis is to provide more methods to evaluate the measurement volume of a NIRS sensor.

Generally, the main goal of this thesis is to enable researchers in the medical field, neurologists in particular, to obtain more extensive information of the

functioning of the brain and the human body. This is done by enabling synchronised simultaneous measurements of blood metabolism and blood pressure in combination with EEG and fMRI. In the long term, this system will contribute toward developing new methods of diagnosing and monitoring brain-related illnesses and disorders. For instance, the developed multimodal measurement system is already utilized to study patients with epilepsy and narcolepsy. More than 70 persons have been examined with this setup.

1.4 Objectives, contribution and novelty of the thesis

The main goal here was to develop a novel biomedical multimodal measurement setup that enables simultaneous continuous measurement of HR, BP fluctuations and blood metabolism, particularly in the brain, during fMRI and EEG. This required ensuring the MRI-compatibility of the measurement methods and of the materials used in the instruments. This is probably the only multimodal setup in the world that allows non-invasive, simultaneous and continuous measurement of such a wide range of modalities, including fMRI, EEG, expCO₂, SpO₂, ECG, NIBP and fNIRS. Of these, the author has contributed on the last two modalities. Development of the fNIRS device was started in cooperation with Hannu Sorvoja, while further development was mostly conducted with Vesa Korhonen. Others who greatly contributed to the development of the NIBP measurement method include Juha Harja and Aleksandra Zienkiewicz, who worked on data processing. Prototyping and further development of the devices has taken several years. Some trainee students took part in this work under my guidance and are mentioned in the Acknowledgement sections of the papers they worked on. A particularly important contribution was made by Mikko Koutonen in relation to the NIRS device. At present, this multimodal setup is in use in the Department of Diagnostic Radiology at Oulu University Hospital, where the setup was built by the author, together with Vesa Kiviniemi, Vesa Korhonen and Tuija Hiltunen.

Another challenge was to validate the developed measurement methods, related to NIBP and fNIRS. One challenge involved estimating light penetration within brain tissue, particularly the maximum achievable penetration depth of the developed NIRS device. This was done *in vivo* by measuring the intensity of back-scattered light at different distances from the light source and by using a novel optical phantom measurement setup, presented in Paper VII. The utility and thereby the validity of the developed methods are emphasized in Paper VI, in which they are put through their paces in a clinical setting.

In the following list are some separate objectives that were considered during this thesis work, covering a time span of more than seven years.

1. Study of MRI-compatibility requirements related to medical instrumentation and data transfer, including measurements of the electromagnetic fields produced by the MRI scanner.
2. Development of methods to perform continuous non-invasive measurement of fluctuations of BP and blood flow in different parts of the human body during MRI.
3. Development of an expandable fibre optic measurement method that utilizes LEDs to measure fluctuations in blood oxygen levels in the brain cortex during MRI scanning. The method is intended to be as convertible as possible, to allow application to the study of other issues related to blood and tissue metabolism, in conjunction with MRI.
4. Realizing and testing the novel multimodal measurement setup and conducting clinical measurements with the entire system in the MRI-environment. Medical data analysis is excluded from the thesis.

In addition to the large number of different multimodalities, one novelty provided by the setup is the possibility to continuously estimate blood pressure changes during MRI. One significant contribution related to the developed NIRS device is the ability to use a wide range of wavelengths in a compact MRI-compatible device, which allows studying metabolism using different combinations of wavelengths, rather than just measuring oxygenation changes. Additional advantages offered by the compactness of the device include not only MRI-compatibility, but also portability and the possibility to implement wearable applications in near future, thereby enhancing the range of possibilities to conduct medical studies by the system.

1.5 Outline of the thesis

This thesis is organized as follows: Section 1 presents the background of the used measurement methods, followed by a description of the motivation and objectives of the thesis. Section 2 is devoted to the extraordinary MRI measurement environment, explaining the limitations and restrictions that need to be considered when conducting measurements in this environment or developing new instrumentations and devices for it. Objective 2 in particular is discussed in Section 2, but also in papers I, II and III. Section 3 explains the developed

measurement methods and presents the novel multimodal setup. Objective 2 is covered in Section 3.2 and in papers III, IV and V, while Objective 3 is at the core of Section 3.1. and Paper II, with a specific focus on the principle of the measurement method. Also papers VI and VII relate partly to Objective 3. Finally, realization of the system and the process of conducting measurements are shown in Section 3.3. (Objective 4). Moreover, results validating the measurement methods are shown in Section 4, providing a basis for Section 5, which discusses the limitations and accuracy of the measurement methods and the multimodal setup. It also suggests possible improvements to the methods and discusses light propagation in the context of brain measurements as well as the accuracy of PTT, before tackling current and future work with the multimodal setup. Section 6 concludes the thesis.

2 MRI room as a measurement environment

Magnetism is a property that indicates how a material responds to an applied magnetic field. Some materials, known as non-magnetic substances, are practically insensitive to magnetic fields. This group includes materials such as aluminium, copper and plastic. However, most materials are influenced by the presence of a magnetic field. Some materials are attracted to a magnetic field, while others are repulsed by it. The first group is referred to as paramagnetic materials and the latter as diamagnetic materials. However, substances can also have a more complex relationship with an applied magnetic field. A detailed explanation of magnetism and how different materials are influenced by a magnetic field can be found, for example, in the book by (Carmen-Gabriela 2012).

2.1 Electromagnetic interference (EMI) and MRI compatibility

Inside the MRI room, a large static magnetic field is on all the time to set protons in the scanning object in a stable state. This poses high demands on the materials and devices used in the room. Most importantly, they cannot contain ferromagnetic materials that would be affected by the magnetic fields. Forbidden are such materials as iron and steel, but metals like aluminium, brass, copper and titanium are allowed. This is a highly relevant consideration when selecting materials and designing electronics, connectors and enclosures (Dyer 2006, I, II and III). Also, due to safety reasons, objects made of ferromagnetic materials are not allowed to be brought into the chamber, as they could cause a fatal attraction, where, for example, sharp objects, like scissors, could hit a person's head inside the MRI tube. As a matter of fact, these kinds of accidents have been reported to happen. Because of the many potential risks in the MRI environment for patients and personnel, guidance documents on MR safe practices are available. Among these, the MRI safe practices guidelines of the American College of Radiology (ACR), initially published in 2002, have become the de facto standard for safe and responsible practices in clinical and research MRI environments (Expert Panel on MR Safety 2013).

In addition to a static magnetic field, the scanner produces an electromagnetic field in the MHz range to excite protons. Moreover, switched gradient fields are pulsed in the kHz range to provide spatial information for images (Rinck 2013). As a result, when the scanner is on, electromagnetic interference in its vicinity

typically appears in a wide frequency range, from ~ 0 Hz to 1.5 GHz (I). Therefore, devices used inside the MRI room must be electromagnetically sealed to prevent electromagnetic radiation from entering or escaping the enclosure. However, in some cases, depending on the measurement method, some parts of a device, the sensors, for instance, cannot be placed inside an enclosure (II, III). This may significantly complicate device implementation.

2.2 Placement of the instruments and devices

There are restrictions as to where devices and components can be placed inside the MRI room. Different restriction zones are normally marked on the floor by the manufacturer of the MRI system. These zones are at specific distances from the scanner, determined by the strength of the magnetic field, and can be used to guide device placement. Fig. 1 illustrates different zones marked inside an MRI operating room housing a 3-Tesla strength closed MRI scanner.

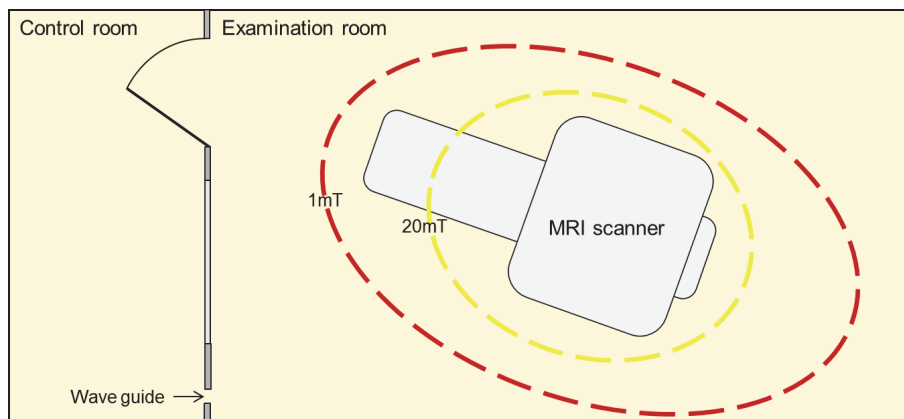


Fig. 1. An MRI operating room typically has markings on the floor indicating different static magnetic field zones that need to be observed when placing devices within the room. The figure presents a floor plan illustrating 1mT and 20mT static magnetic field zones marked around a 3T MRI scanner, based on the manufacturer's manual. In addition, the walls of the chamber are RF-shielded. Possible holes in the walls, shown on the lower left corner, are realised as waveguides to prevent electromagnetic interference from penetrating to the other side of the room.

Naturally, devices placed further from the MRI scanner, as shown in Fig. 2, have less stringent MRI-compatibility requirements, as long as their shielding is

properly done. Hence, medical devices and implants are categorized according to (ASTM International 2005) to the following classes: 1) MR safe, for completely non-magnetic, non-electrically conductive, and non-RF reactive devices and implants, 2) MR conditional, may contain magnetic, electrically conductive or RF-reactive components that is safe for operations in proximity to the MRI and 3) MR unsafe, for objects that pose a clear and direct threat to persons and equipment inside the MRI room.

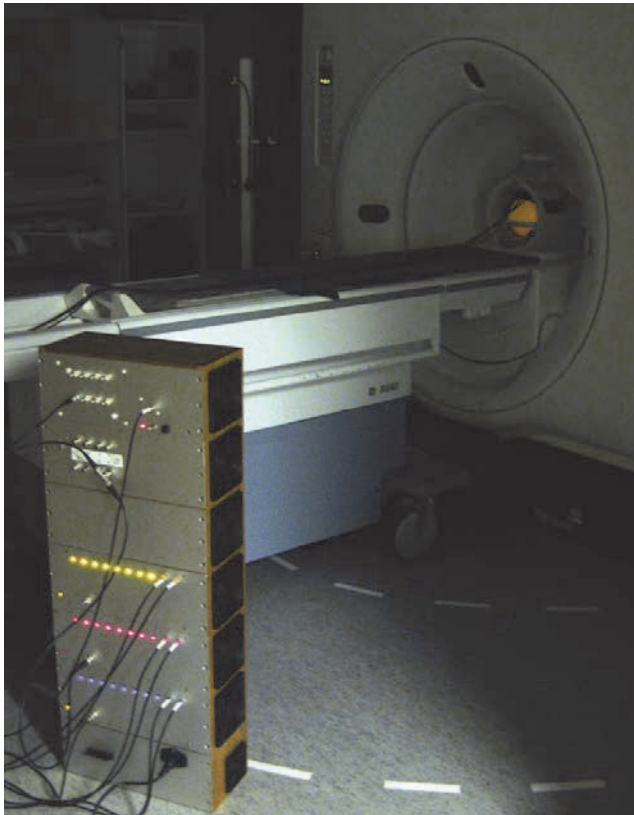


Fig. 2. MRI-compatibility tests of the developed NIRS device. A calibration phantom, visible in the figure as a yellow ball inside the MRI scanner, is illuminated using fibre bundles. Attached on its surface are fibre optodes. To avoid disturbance, the device containing electronic parts is placed further from the scanner. Please, note the different static magnetic field zones marked on the floor. (Paper II, published with the permission of © 2010 Turpion-Moscow Ltd).

Due to MRI-compatibility issues, a sound approach to device placement involves placing only essential device components and units inside the MRI room itself, provided that it is possible to implement the interface of the units between the control and the examination rooms. The interface and cabling can be realized, for example, by waveguides, which are commonly found in the RF-shielded walls of the MRI room. Although the main purpose of the waveguides is to allow fluid flows into the MRI room, including air conditioning, water and medical gases (ETS Lindgren 2009), they can, nonetheless, be used for short-term fibre cabling purposes to enable data transfer during measurements. If electrical cables are used, special attention must be paid to proper filtering. Naturally, if the setup is intended to be used as a stationary measurement system, it is preferable to use solid through-the-wall cabling.

2.3 Data transfer inside the MRI room

Optical fibres are the most feasible data transfer method for the MRI environment, because fibres can easily be made MRI-compatible and the light they carry is not affected by magnetic fields. Moreover, they can be placed directly inside the scanning volume of the MRI scanner (II and III). Further away from the scanner, it is possible to use electrical cables made from copper, as long as they are well-shielded and all the materials are MR-compatible. In such cases, to ensure MRI-compatibility, the minimum distance from the scanner can be determined only by test measurements using an MRI calibration phantom.

Paper (I) explored the possibilities of using wireless data transfer in the MRI environment, particularly by testing wireless short range devices (SRD) inside the MRI room at different distances from the scanner. Wireless data transfer has become commonplace also in hospitals. Radio frequency (RF) fields, generated, for example, by mobile phones, cannot be avoided, since they are ubiquitous. Different types of local wireless data transfer techniques are used everywhere in the hospital environment, including wireless local area network (WLAN) and Bluetooth. Moreover, radio frequency identification (RFID) is increasingly being exploited in health care for tracking applications, to track components and assets and to monitor patients. In addition, wireless body area networks are being introduced, and will probably come into common use in the near future. These applications may also include implants used within the human body. At present, wireless techniques do not pose a specific problem to medical devices, since they are compatible with existing wireless data transfer protocols and comply not only

to electromagnetic compatibility (EMC) standards but, on demand, also to the specific requirements of medical use. However, the MRI room remains an environment, where wireless techniques are not yet used and even the possibilities remain largely unexplored. To remedy that deficiency, this thesis experimentally investigated wireless data transfer, particularly its effect on MRI scanning and, vice versa, the effect of MRI scanning on the reliability of wireless data transfer in the MRI room (I), shown in Fig. 3.



Fig. 3. Test setup in the MRI room. Wireless SRDs are placed on the table near the MRI scanner (Paper I, published with the permission of © 2007 by University of Oulu).

To that end, the following test scenarios were used:

- Electromagnetic field in the MRI room was measured with the scanner on, while one transceiver at a time was sending test data.
- Also tested was the situation in which the scanner and all the different transceivers were on at the same time.
- In addition, effect of MRI scanning on the reliability of the wireless link between transceiver pairs was observed.

Based on our on-site measurements, it seems that use of wireless short-range data transfer in a hospital's MRI operating room is possible, although the measurements indicate that the EMI produced by an MRI scanner is significant over a very wide frequency range, between ~ 0 Hz and 1.5 GHz. Shown in Fig. 4 is EMI produced by a 0.23T scanner (Philips Medical Systems MR Technologies Finland Inc., Vantaa, Finland) during scanning. If the transceivers' operating frequency band is above 1.5GHz, then MRI has no effect on the radio link. Fig. 4 shows a Bluetooth link at a frequency of approximately 2.4 GHz, which is above the interference frequency range.

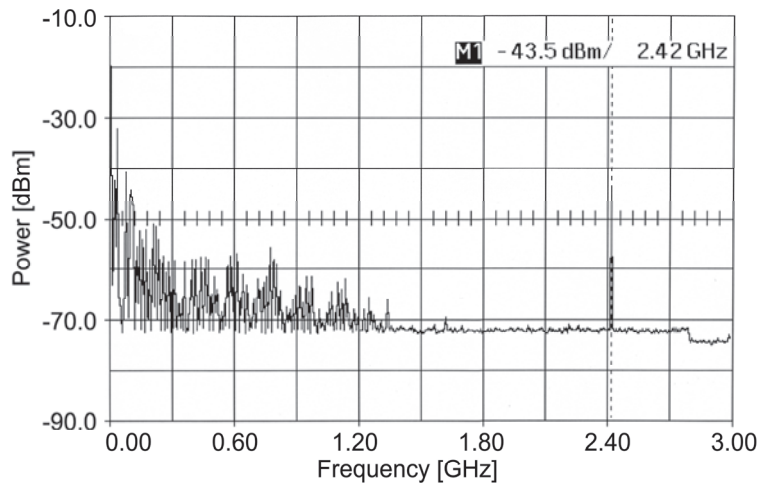


Fig. 4. EMI spectrum produced by 0.23T scanner measured inside the MRI room. Inside the MRI room one Bluetooth transceiver was active showing a peak near at frequency of 2.4GHz. (Paper I, published with the permission of © 2007 by University of Oulu).

Results of the EMI measurements were additionally exploited to design RF shielding for the NIRS device. Because interference caused by the scanner is limited to frequencies of less than 1.5 GHz, and we suppose that this frequency corresponds to a wavelength of approximately 20 cm, the device enclosure must not have holes larger than, roughly, one tenth of that without a dramatic loss of shielding effectiveness. Since dissipated power must be blown out through the device enclosure, holes are unavoidable. Despite that, high shielding effectiveness can be achieved by screen plates with small holes in their ventilation outputs.

Studies related to the MRI room as an environment for measurement design and possible interference issues have been covered, for example, in the following publications (Virtanen 2006; Niendorf *et al.* 2012).

3 Methods of measurement and the multimodal setup

Developing a multimodal measurement setup for the MRI environment has taken several years of close cooperation between the Optoelectronics and Measurement Techniques (OEM) Laboratory at the University of Oulu and the Oulu Functional Neuroimaging (OFNI) group based at Oulu University Hospital, both located in Finland. At the present time, the setup consists of seven independent measurement and imaging modalities that can be used simultaneously and in synchrony. Importantly, responses gathered with the different methods are not influenced by each other. This multimodal setup, called *Hepta-scan*, allows the continuous simultaneous measurement of respiration, HR, electrical activity in the human brain and metabolism of the brain and peripheral tissue as well as pulse wave velocity (PWV) and BP measurements in synchrony with MRI.

Two non-invasive optical measurement methods, developed particularly for the setup, will be presented in this section. The first is based on near-infrared spectroscopy (NIRS) to monitor blood metabolism and the other on using acceleration and optode sensors to monitor HR, PWV and BP fluctuations. All sensors used in the measurement methods are non-invasive and safe for the patient.

3.1 Optical NIRS-based measurement method to monitor metabolism and blood flow pulsations during MRI

Because of cortical neural activity, proportions of HbO₂ and Hb change endogenously. Such oxygenation changes can be accurately monitored in the time domain by fNIRS-based measurement methods. As mentioned earlier, although fMRI only allows monitoring brain oxygenation fluctuations with low time resolution, it has the advantage of high spatial accuracy, on the order of less than a millimetre. fNIRS, on the other hand, has modest spatial resolution due to extremely the high scattering rate of light in biological tissue and the optical heterogeneity of the human head (Toronov *et al.* 2007). However, by combining data responses from these two modalities, it is possible to measure oxygen level fluctuations in the cortex with high spatial and temporal resolution. To enable this, the MR-compatibility of fNIRS measurements was one of our main priorities in device development. Other priorities were cost-effectiveness, portability and

convertibility, to allow the application of different wavelength combinations, determined by the purpose of each measurement.

3.1.1 Utilization of high power LEDs in illumination

A study by Okada revealed that to reach the grey matter layer of the brain in NIR reflectometry, the source-detector separation should be larger than 30 mm (Okada *et al.* 1997). Our phantom measurements (VII) verified that also the measurement method presented here requires a source-detector distance in excess of 3 cm to enable sensing of pulsating liquids behind the grey matter layer, located approximately at a depth of 20 mm from the skin surface on the forehead. Similar results were also observed in our recent paper on the estimation of light propagation in the brain on the basis of Monte Carlo (MC) simulations, phantom and *in vivo* measurements (Korhonen *et al.* 2014). With a source-detector separation of over 30 mm, near-infrared light back-scattered from tissue will be significantly attenuated before reaching the detector. Depending on wavelength, this attenuation is approximately 8 orders of magnitude (II). Similar results were accomplished in Paper (VII) in conjunction with phantom and *in vivo* measurements.

Owing to high attenuation and scattering of light, common measurement methods based on NIRS tend to employ lasers or laser diodes (LD). They enable sufficient illumination power to reach the cerebral cortex and allow measuring the back-scattered light with a good signal-to-noise ratio (SNR). On the other hand, there are also limits for improving the SNR by increasing illumination power. First of all, *in vivo* medical measurements require strict safety considerations with regard to optical power levels. Secondly, the measurement result may be affected by possible tissue warming (Strangman *et al.* 2002). This is a particularly relevant concern for continuous *in vivo* measurements, where the measurement time and, consequently, illumination, is long.

In recent years, the obtainable optical output power of LEDs has also reached a level that is sufficiently high for sensing the cerebral cortex. Additional factors contributing to a more effective utilization of LEDs include improvements in stability and widening of the available spectrum. In the interest of cost effectiveness, portability and easy irreplaceability, determined, for instance, by the wavelength of interest, we decided to implement the device using high-power LED (HPLED) technology instead of laser technology (II). Nowadays, HPLEDs can be driven at a maximum current of several amperes, provided that they are

well-connected to heat dissipation. Moreover, for NIRS measurements, a good selection of wavelengths with sufficient output power is now available in the near-infrared range, as shown by Table 1.

Table 1. Examples of commercially available LEDs in 2014, with wavelengths of interest and their output powers. The cited power values are taken from datasheets by Osram, Roithner LaserTechnik and Thorlabs.

Wavelength [nm]	Output power [mW]
940	550
905	400
850	630
760	370
678	550
660	650

Another advantage of using LEDs is that they are small in size and can be accommodated in an area of less than 2 cm², see Fig. 5. Ultimately, the compactness of the final device depends largely on the cooling system required by the high operation currents (II). Fortunately, the packaging design of HP LEDs allows attaching a variety of cooling plates.

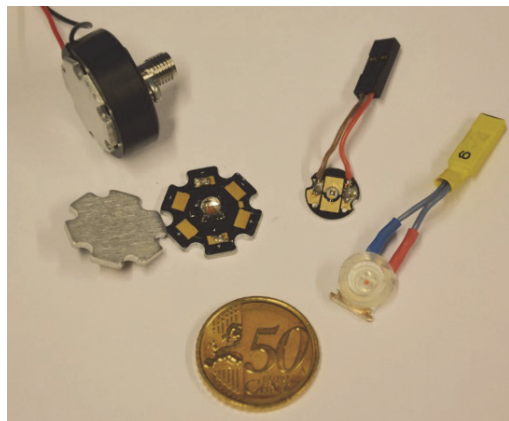


Fig. 5. Example of HP LEDs next to a 50 cent coin for comparison. Seen in the upper left corner is a LED, similar to the LED shown in the middle, attached on a female SMA connector for fibre coupling.

3.1.2 Lock-in amplification for detecting and separating different wavelengths

Owing to strong absorption and attenuation of light in tissue and, to a lesser degree, to attenuation in connectors and fibres (Myllylä *et al.* 2011), the optical output power of HPLEDs is high. Nevertheless, the power levels of light to be detected are in the nano- and microwatt range. Consequently, one challenge in developing the device involved focusing on receiving a sufficient signal to obtain information from deep within tissue. Additionally, for this kind of measurement application, small changes in light intensity are of specific interest. As a result, it was infeasible to use the CW method to monitor the brain cortex with LEDs. In the same vein, the TR method was impracticable, because LEDs cannot accurately produce short pulses on the picosecond scale. We decided, therefore, to implement a modulation-based technique, the FD method, mentioned in Section 1.2.1. Moreover, signal amplification in the developed device is based on lock-in amplification, where instead of amplification of the received signal at the whole frequency band of interest, only amplitude-modulated light signals at a specific narrow modulation frequency band are amplified. As a result, a significant increase in SNR performance can be achieved. This allows attaining optimal reduction of noise generated by different sources, particularly when using well-matched amplification and filtering (II).

Fig. 6 presents the basic principle of the measurement method utilized in the developed device. Thanks to its four modulation channels, the device has the capacity to simultaneously measure four wavelengths/LEDs. Each LED/wavelength is driven by a specific modulation frequency and light is emitted into tissue by a *4 input to 1 output* fibre bundle, Fig. 7. Light that is back-scattered from tissue is received by a fibre detector, and the light signal, transduced to a current, is amplified and band pass filtered. Next, each signal is demodulated, i.e., multiplied by a lock-in reference signal (ref.). These reference signals operate at the same frequencies as the LEDs. The signals can be taken directly from the modulator or by measuring the LEDs' outputs by detectors - this allows taking into account instabilities in the LED output, caused by heating or noise, for instance. Finally, the demodulated signals are low-pass (LP) filtered and amplitude changes in the remaining output signal are correlated with intensity changes of the received light signal at specific wavelengths. Lock-in amplification enables separating several wavelengths from each other, because

each LED/wavelength is labelled with a specific modulation frequency. Hence, the technique is well-suited for fNIRS-based measurements.

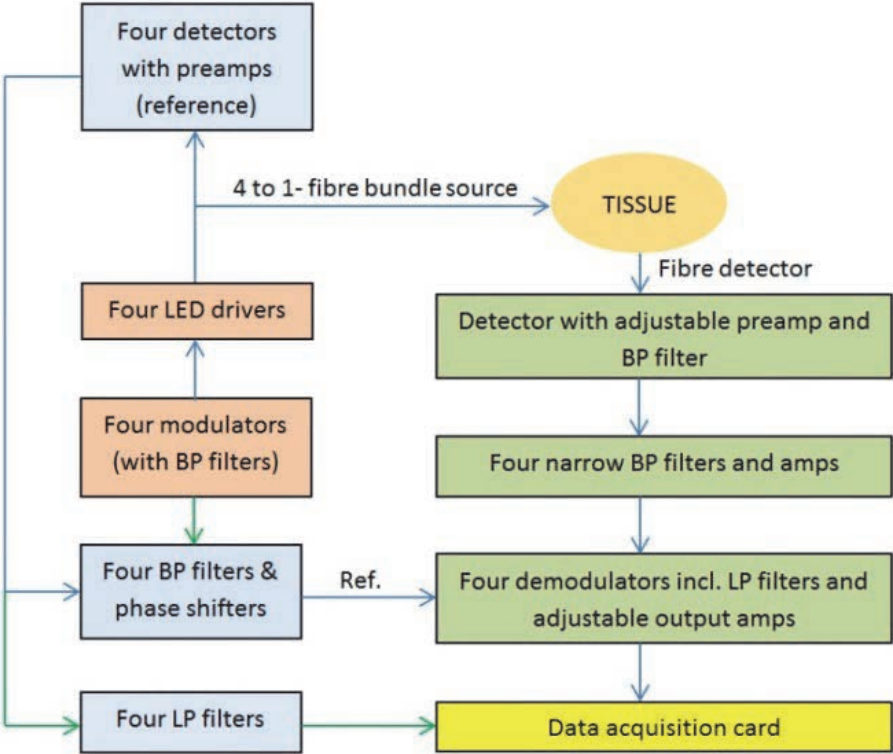


Fig. 6. Principle of the NIRS measurement system using lock-in amplification. As seen, the system employs four different wavelengths. In this figure, BP stands for band pass and LP for low pass.

The output power of the LEDs is collected by an MRI-compatible fibre bundle with four inputs, shown in Fig. 7. After mixing the four wavelengths, the output of the fibre serves as the fibre source to illuminate the tissue under study. Bent to a 90 degree angle, the fibre output tip has a thickness of 2.5 mm. Thanks to bending, the fibre tip is practical for achieving good skin contact, as it can be pushed tightly on the skin and as hair does not easily get in the way to block the signal.



Fig. 7. Fibre bundle with four inputs (male SMA connectors). Light from the four sources is guided to one fibre output with a 90 degree bend. The diameter of the fibre tip is 2.5mm.

Shown in Fig. 8 are two versions of fibre attachment. In the solution on the left, back-scattered light is received by two fibre detectors at a distance of 5 mm and 30 mm, respectively, from the fibre source. The shorter distance is used for comparison, giving pulsations measured from the skin, while the other detector measures pulsations from the brain cortex. The other version, made of flexible rubber, has 5 detectors.



Fig. 8. Fibre clips. On the left and upper right corner, a source fibre and two detector fibres attached at a distance of 5mm and 30 mm, respectively, from it. On the lower right corner is shown a clip version, made of flexible rubber, with five detectors. The thickness of the fibre output is 2.5 mm, and it is bent to a 90 degree angle.

AM is quite easy to implement with LEDs, since their output power is linearly proportional to the drive current. However, a typical LED can only generate frequencies below one MHz, when transmitting at a high power level. This must be taken into account in the selection of modulation frequency. Moreover, it limits the range of possibilities in using phase detection to determine the optical path between the source and the detector. On the basis of these considerations, the developed device relies on mean values from literature to determine the optical path. However, the spatial accuracy of the method can be improved by the use of several detectors, related to spatially resolved spectroscopy (SRS).

Commonly, the shape of the modulation signal used in the lock-in technique is sinusoidal or rectangular. With rectangular waves in particular, the spectral power expands to higher frequencies; the corner frequencies will be at $1/\text{phi} \cdot T$ and $1/\text{phi} \cdot t$, where T is pulse width and t the rise or fall time of the pulse. In the case of a 50% duty cycle, only even harmonic waves will be formed. If the duty cycle is less or more than that, also odd modes will be formed. One way of countering this involves using lower rise and fall times. A sinusoidal modulation signal, in contrast, does not produce any harmonic frequencies, provided that the waveform is perfectly sinusoidal without any distortion (Wang *et al.* 2011). However, in reality, harmonic distortion is always present in both wave shapes, since ideal signal waves are impossible to generate. Additionally, application of several modulation frequencies gives rise to intermodulation distortion. As harmonic or other types of distortion spread power to other frequencies, they produce noise and unnecessary heating of the LED. Modulation signals tend to be modulated by square waves, rather than sinusoidal ones, since they are easier to produce accurately (Schofield 1994). Furthermore, when several wavelengths are generated by different LEDs, modulation frequencies have to be carefully selected and accurately band-pass filtered to avoid crosstalk between the different wavelengths (Myllylä *et al.* 2013).

Phase-sensitive detector

Based on using a phase-sensitive detector (PSD), the selected method demodulates the received amplitude modulated (AM) signals of a specific frequency by reference signals with the same frequency. Fig. 9 presents the basic principle of demodulation.

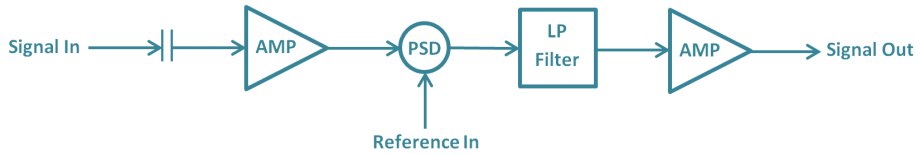


Fig. 9. Principle of PSD and lock-in amplification.

For sinusoidal modulation, AM signals can be mathematically expressed using the following equations:

$$V_I(t) = V_0 \sin(\omega t + \phi) \quad (1)$$

$$V_R(t) = \sin(\omega_R t) \quad (2)$$

Shown in Fig. 9, the input signal $V(t)$, with a phase ϕ , passes through a capacitor, which removes a possible DC offset from the signal. Thereafter, it is amplified by AMP and then multiplied by the reference signal $V_R(t)$ at the known phase difference between the two signals, using a PSD. The result of the multiplication can be expressed as Equation (3).

$$V(t)_I V_R(t) = \frac{V_0}{2} \{ \cos[(\omega - \omega_R)t + \phi] - \cos[(\omega + \omega_R)t + \phi] \} \quad (3)$$

Further, if both the input and reference signals have the same frequency, the equation can be expressed as follows:

$$V(t)_I V_R(t) = \frac{V_0}{2} \{ \cos[\phi] - \cos[2\omega t + \phi] \}, \omega = \omega = \omega_R \quad (4)$$

Thus, when adjusting the phase, a direct value can be provided for the signal amplitude of $V(t)$ by the DC component of this product (Schofield 1994).

Signal demodulation can be either hardware or software-based. A common type of software-based demodulation involves using LabView, while hardware-based demodulation can be performed, for example, by a high-precision balanced modulator/demodulator, such as the AD630, by Analog Devices. Software-based signal processing is advantageous in terms of developing a new measurement method, because it allows modifications. It is also easy to add different indicators between blocks in the signal processing path, thus enabling measurement optimization by monitoring the signal processing path (Myllylä *et al.* 2011). For example, the frequency, phase and amplitude of both the received and the reference signal can be simultaneously observed during signal processing.

However, the used data acquisition (DAQ) card requires a high sampling rate to enable acquisition of modulated signals with sufficient accuracy. This reduces the number of modulated wavelengths and channels that can be measured simultaneously.

3.1.3 Quantifying tissue metabolism on the basis of received signals

When light penetrates into tissue, it starts to scatter and attenuate (Tuchin 2007, Popp *et al.* 2012). This event is also affected by partly irregular physiological events, such as breathing, muscle movements and blood flow. The result is that intensity changes in the frequency spectrum of the received light exhibit constant nonlinear variation. Most importantly, these intensity changes also include wavelength-dependent variation that can be exploited to monitor metabolism and brain activity (Madsen 2013).

Fig. 10 shows the relative absorption spectrum for water, Hb, HbO₂, cytochrome and melanin measured at wavelengths between 500 nm and 1000 nm. Concentrations of these substances in tissue can be optically determined using a relative spectroscopic measurement at two or more near-infrared wavelengths. In terms of brain activity monitoring, the chromophores (molecules that absorb light) of most interest are haemoglobin and cytochrome Caa3, because concentration of these chromophores varies with time and oxygenation status (Elwell & Phil, 1995). By looking at Fig. 10, it can be seen that changes in cytochrome Caa3 (oxidized) and cytochrome Caa3 (reduced) reflect oxygenation status in a manner similar to Hb and HbO₂. When measuring haemoglobin concentration, cytochrome Caa3 does not show a significant effect, because its attenuation is an order of magnitude lower than that of haemoglobin (Madsen *et al.* 1999). By the same reason, measuring cytochrome Caa3 concentration is a much more difficult undertaking. Possibilities of determining the concentration of cerebral oxidized cytochrome have attracted some attention, because it can be used to measure changes in mitochondrial oxygen delivery and as an ischemic threshold (Cope *et al.* 1991, Tsuji *et al.* 1995, Cooper *et al.* 1997 & 1999, Tisdall *et al.* 2007). Of particular interest in Fig. 10 are the isosbestic points, i.e., the specific wavelengths at which the absorptivity of two chromophores is equal. For instance, at approximately 740 nm, the isosbestic point for cytochrome Caa3 (oxidized) and cytochrome Caa3 (reduced) is at a different wavelength than the isosbestic point for Hb and HbO₂.

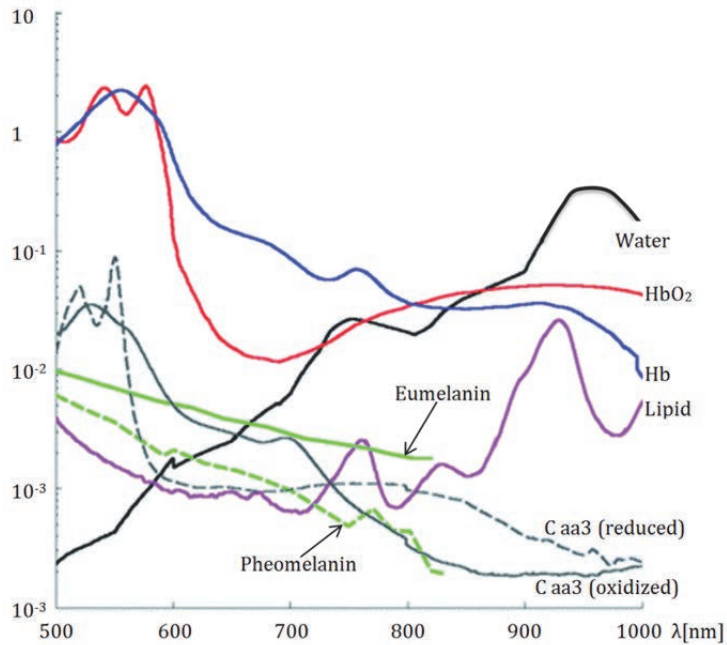


Fig. 10. Relative absorption spectrum for water, haemoglobin etc. as a function of wavelength, adapted from (Madsen 2013).

The most common NIRS measurement involves quantifying concentrations of Hb and HbO₂. This is usually done by comparing the light absorption of two wavelengths on both sides of their isosbestic point, at approximately 800 nm. Fig. 11 shows typical optical absorption spectra for HbO₂ and Hb. The figure also presents additional wavelength spectra of several HP LEDs, which can be used in the developed device. Appropriate wavelengths are selected on the basis of the substances whose concentrations we are currently interested in measuring. For example, if the focus is on establishing the concentration levels of Hb and HbO₂, we choose a pair of LEDs, of which the first one has a wavelength shorter than 800 nm and the other a wavelength longer than that.

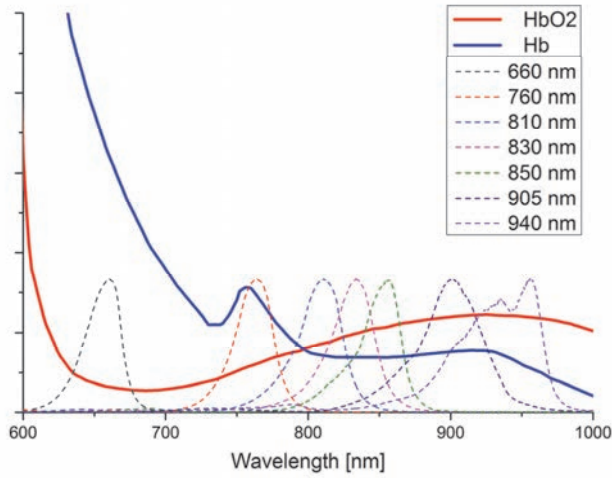


Fig. 11. Estimated optical absorption spectra for HbO₂ and Hb. Also shown are measured optical output spectra of certain HPLEDs used in the experiments, placed within the spectrum of interest.

When light with a constant intensity penetrates ($I_{initial}$) into tissue, the back-scattered light that is detected ($I_{detected}$), is attenuated by chromophores. Furthermore, attenuation changes occur as a result of changes in chromophore concentration, which can be recorded as wavelength-dependent changes in the intensity of the detected light. Moreover, changes in chromophore concentration are linearly related to changes in the logarithm of the detected light. This relationship, called optical density (OD), is known as the Beer-Lambert law, shown in Equation (5), named after August Beer and Johann Lambert (Wyatt *et al.* 1990, Boas *et al.* 2001, Willmann *et al.* 2003).

$$OD = -\log \frac{I_{detected}}{I_{initial}} \quad (5)$$

By using Expression (6), we may determine the concentration of a substance [X], when a photon with a known path length L penetrates through it and a change of OD is measured

$$\Delta OD = \varepsilon \cdot [X] \cdot L \quad (6)$$

where ε is the wavelength-dependent molar extinction coefficient for the compound, describing the amount of light it absorbs. Figs. 21 and 22 show that

intensity of collimated light decreases non-linearly and exponentially as a function of penetration depth. The coefficient of this exponential decay is known as the absorption coefficient μ_A , for samples with multiple absorbing compounds, as in Equation (7)

$$\mu_A = \sum_{i=1}^N \varepsilon_i \cdot [X_i] \quad (7)$$

where ε_i is the extinction coefficient and $[X_i]$ the concentration of the N number of compounds.

Not being a homogenous substance, tissue, in addition to attenuation, also causes light scattering. As a result, light diffuses within it and some parts of light travel a longer path than others, before reaching the detector. Needless to say, light with a longer path tends to be more attenuated. Also changes in the intensity of the received light are affected by the additional path length. The scattering coefficient μ_S is also an exponential coefficient related to the scattering probability of a photon per unit length and is generally several orders of magnitude larger than μ_A , which means that light scatters many times and changes its direction at each absorption event. Moreover, the anisotropy factor g is defined as the average of the cosine of the difference between the incident angle and direction after a scattering event. The reduced scattering coefficient μ'_s includes the scattering coefficient and the anisotropy term and can be calculated from Equation (8) (Madsen 2012).

$$\mu'_s = \mu_s \cdot (1 - g). \quad (8)$$

Different layers of brain tissue have different optical properties, described by the coefficients μ_A , μ_S and g . These are used in MC simulations and in the fabrication of phantoms for different tissue layers, as described in Papers (II and VII). Optical properties of human tissues measured *in vivo*, *ex vivo* and *in vivo* can be found, for example, in book by (Tuchin 2007).

The modified Beer-Lambert (MBLL) law takes account of the scattering effect, by averaging the path length of light through tissue on the basis of constant scattering losses (Delphy *et al.* 1988). MBLL is described precisely in many publications (Cope *et al.* 1988, Schelkanova *et al.* 2011). The equation can be written as follows:

$$\Delta OD = \mu_A \cdot L \cdot DPF + G \quad (9)$$

where L is the distance between the source and the detector, now corrected by a constant factor DPF (differential path-length factor), taking into account the increase in path length. G is the constant geometry factor. OD and DPF are specific for each wavelength of light.

In general, at least one wavelength must be recorded for each unknown chromophore to provide an estimation of its concentration. In the estimation of Hb and HbO₂, the MBLL is given by the following equation:

$$\Delta OD^\lambda = (\epsilon_{HbO_2}^\lambda \Delta[HbO_2] + \epsilon_{Hb}^\lambda \Delta[Hb]) \cdot DPF^\lambda \cdot L \quad (10)$$

where λ indicates the particular wavelength used in the measurement. As already stated, for Hb and HbO₂, at least two wavelengths are required. Equation (10) allows calculating independent concentration changes in Hb and HbO₂. For this, ΔOD has to be measured for two wavelengths λ_1 and λ_2 , and by using the known extinction coefficients of Hb and HbO₂ for these wavelengths, the concentration changes can be solved using the following equations:

$$\Delta[Hb] = \frac{\epsilon_{HbO}^{\lambda_2} \frac{\Delta OD^{\lambda_1}}{B} - \epsilon_{HbO}^{\lambda_1} \frac{\Delta OD^{\lambda_2}}{B}}{(\epsilon_{Hb}^{\lambda_1} \epsilon_{HbO}^{\lambda_2} - \epsilon_{Hb}^{\lambda_2} \epsilon_{HbO}^{\lambda_1}) L} \quad (11)$$

$$\Delta[HbO] = \frac{\epsilon_{HbO}^{\lambda_1} \frac{\Delta OD^{\lambda_2}}{B} - \epsilon_{HbO}^{\lambda_2} \frac{\Delta OD^{\lambda_1}}{B}}{(\epsilon_{Hb}^{\lambda_1} \epsilon_{HbO}^{\lambda_2} - \epsilon_{Hb}^{\lambda_2} \epsilon_{HbO}^{\lambda_1}) L} \quad (12)$$

where ΔOD^λ represents change in optical density at a particular wavelength and ϵ is the wavelength-dependent extinction coefficient of the chromophore of interest. There are also modified methods of estimating Hb and HbO₂, some of which are discussed for example in (Ye *et al.* 2009).

Although the MBLL Equation (7) describes the absolute absorption and concentration of chromophores in tissue, in reality, the quantification of absolute concentration is very difficult, due to uncertainties in the values of DPF and G and the presence of other chromophores. This makes a direct quantification of Hb and HbO₂ difficult (Madsen 2012).

3.2 Continuous measurement of BP pulsations during MRI

As already mentioned in Introduction, use of non-invasive methods allows us to continuously measure fluctuations in BP generated by each heart pulse. However,

existing non-invasive methods still cannot provide reliable, accurate absolute BP values. Fortunately, in the study of brain function, often based on a correlation analysis between BP and brain activities, researchers are interested in fluctuations of BP, and not in accurate absolute values (VI).

In the presented multimodal setup, human heart pulse wave responses are non-invasively measured by two MRI-compatible fibre optic methods (III, IV). Thanks to their MR-compatibility, optical fibres are ideal for sensor design. One of the developed sensors is a specially designed fibre optic accelerometer sensor, shown in Fig 12, while the other one is an optical fibre probe, shown in Fig 13, that senses BP pulses based on waveforms extracted with the PPG method (Spigulis 2005, Allen 2007). The method of estimating BP by measuring PTT is commonly known and described in several publications, including (Yoon *et al.* 2009).

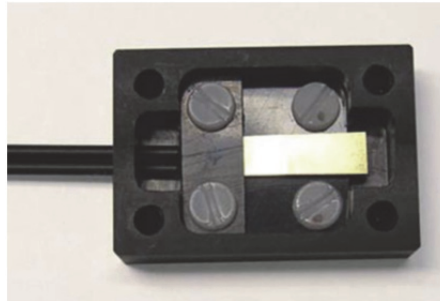


Fig. 12. Fabricated accelerometer. Two fibres, coming from the left, are attached to a cantilever, placed in the middle of the platform box made of polyOxyMethylene plastic. The right side end of the cantilever, made of brass foil, is angled downwards at 90 degrees. (Paper III, published with the permission of © 2011 by WILEY-VCH Verlag GmbH & Co. KGaA, Weinheim).



Fig. 13. Optical probe or optode. Fibre tips of two MR-compatible fibres are on a fibre holder, made of olyOxyMethylene plastic, to provide a stable mounting for fibres at a distance of 5 mm from each other.

Simultaneous use of these two measurement methods enables monitoring the propagation of pressure waves extensively in different areas of the human body (IV). According to our experiences, pulsations from large veins are easier to detect by accelerometers, whereas small veins are easier to sense by optodes with the source and detector near each other. Accelerometers are more sensitive to skin vibrations caused by large veins, while optodes respond to blood flow in small veins within a tissue, both generated by BP.

Accuracy of the time resolution of an optode depends mainly on the source-detector distance (VI), and a time resolution of few milliseconds can be achieved to determine the start of a BP pulse. As for accelerometers, their time resolution is chiefly determined by the mechanical bending properties of the cantilever, particularly by its impulse response and resonance frequency, Fig 14.

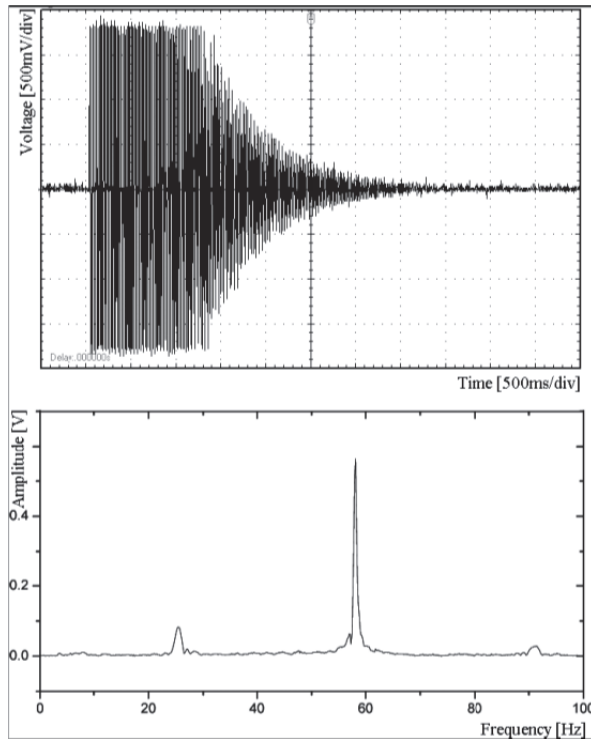


Fig. 14. Impulse response and resonance frequency of the fabricated accelerometer. A resonance frequency of 58 Hz and Q-factor of 129 are sufficiently high for the measurement application. (Paper III, published with the permission of © 2011 by WILEY-VCH Verlag GmbH & Co. KGaA, Weinheim).

3.2.1 Estimation of continuous BP based on pulse wave velocity

In general, the higher the pressure in the aorta, the greater the velocity of blood flow. Because of this mutual relationship between PWV and BP, PWV is a widely used index of arterial distensibility in the estimation of continuous BP (Marcinkevics *et al.* 2009). Using the two presented MRI-compatible fibre optic sensors, PTT values can be calculated on the basis of signals obtained from at least two sensors. These are placed on the chest and the other sensor on neck or on a finger. Also pulse shapes measured by ECG can be used to determine PTT values. Having acquired PTT values from different sensors, it is possible to calculate PWV, provided that the distance between the sensors is known, using the following equation:

$$p_{wv} = \frac{s}{t} \quad (13)$$

However, the thickness of the vessel wall (h), the diameter of the vessel (d) and the density of blood (ρ) also have an effect on velocity. Equation (14) shows a mathematical expression for this dependence, where E stands for Young's modulus, describing the elasticity of the arterial wall (McDonald *et al.* 1974, Hughes *et al.* 1979, III). Naturally, it is very difficult to accurately determine these values, or to measure velocity from a single vessel. Thus, the values used in the equation are estimations. By the same token, the calculated value of PWV is an estimation.

$$p_{wv} = \sqrt{\frac{h \cdot E}{d \cdot \rho}} \quad (14)$$

Moreover, a relationship exists between the elasticity coefficient of the vessel and the pressure P inside it, as shown in Equation (15). This means that BP inside the vessel continuously affects the value of the Young's modulus of the arterial wall E .

$$E = E_0 \cdot e^{\zeta \cdot P} \quad (15)$$

where E_0 is the zero pressure Young's modulus (elasticity), ζ is a constant that depends on the vessel ($1,20 \times 10^4$ N/m² – $1,35 \times 10^4$ N/m²) and e is the mathematical constant 2.71828.

By combining Equations (14) and (15), an estimation of blood pressure can be expressed in the form of Equations (16) and (17).

$$P = \frac{1}{\zeta} \cdot \ln \left(\frac{d \cdot \rho \cdot (PWV)^2}{h \cdot E_0} \right) \quad (16)$$

$$P = \frac{1}{\zeta} \cdot \ln \left((PWV)^2 \right) + \frac{1}{\zeta} \cdot \ln \left(\frac{d \cdot \rho}{h \cdot E_0} \right) = k_1 \cdot \ln \left((PWV)^2 \right) + k_2 \quad (17)$$

Factors k_1 and k_2 can be determined using Equations (18) and (19), if two blood pressures, P_1 and P_2 , and their related pulse wave velocities, PWV_1 and PWV_2 , are measured.

$$k_1 = \frac{\ln \left((PWV_1)^2 \right) - \ln \left((PWV_2)^2 \right)}{P_1 - P_2} \quad (18)$$

$$k_2 = P - k_1 \ln((PWV)^2) \quad (19)$$

Factors k_1 and k_2 can be determined in the multimodal setup by an anaesthesia monitoring device, available in the MRI room, which provides BP values measured by a cuff. As these cuff measurements can be repeated once a minute or less, continued NIBP can be calibrated several times during the measurement to improve the accuracy of the recorded BP values.

3.3 Realization of the multimodal measurement setup

The multimodal measurement setup is currently located in the Department of Diagnostic Radiology at Oulu University Hospital, where a 3-Tesla strength closed MRI scanner provides MRI and fMRI data. Figure 15 shows the multimodal measurement setup that provides, in addition to MRI and fMRI, continuous simultaneous measurement of EEG, expCO₂, SpO₂, ECG, NIBP and fNIRS. Basically, the measurement system can be built in all MRI environments, as long as a waveguide on the RF-shielded wall is available for the fibres, and different measurement systems can be linked with each other for synchronised simultaneous measurements.

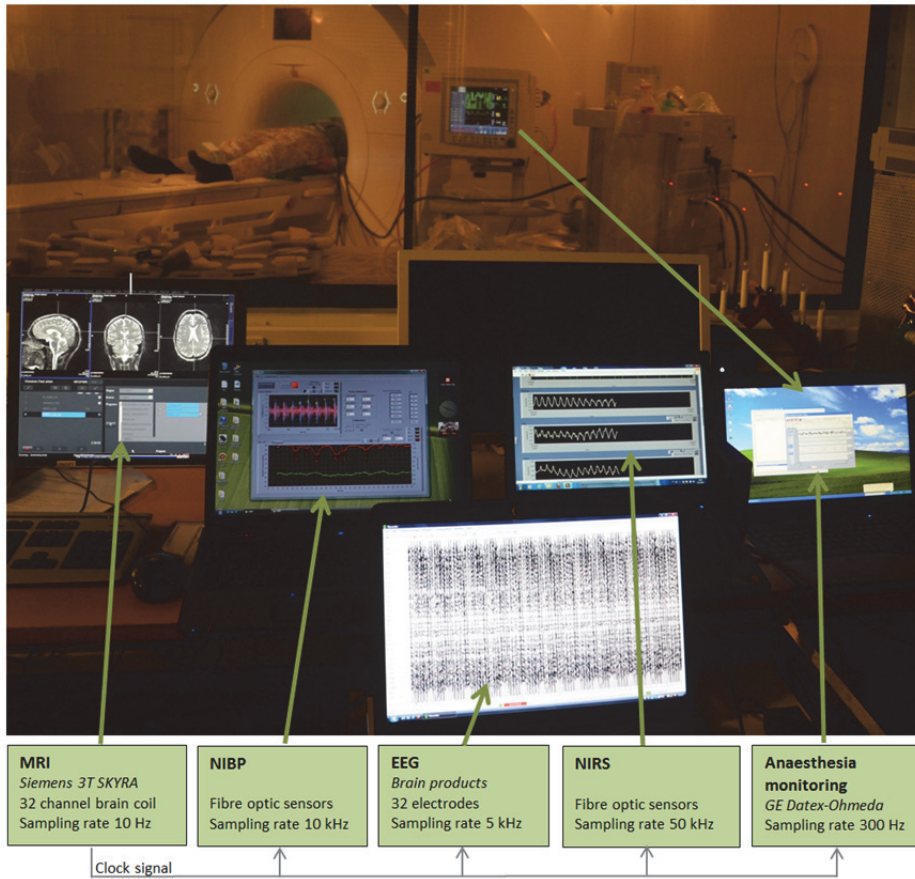


Fig. 15. Setup of the multimodal measurement. Simultaneous measurements include MRI, fNIRS, NIBP and EEG. By using an anaesthesia monitoring device also ECG, CO₂ expiration and oxygen saturation (SpO₂) can be measured.

The body figure illustrated in Fig. 16 shows the sensor attachment positions used in the measurement, while Fig. 17 shows the actual sensor assembly during measurement. However, in this case, the optode sensor was not attached on the toe. All cables coloured in black are optical fibres. The anaesthesia monitoring device on the right is measuring ECG, CO₂ expiration, SpO₂ and BP (by cuff occlusion) at the desired interval of 1 minute or more.

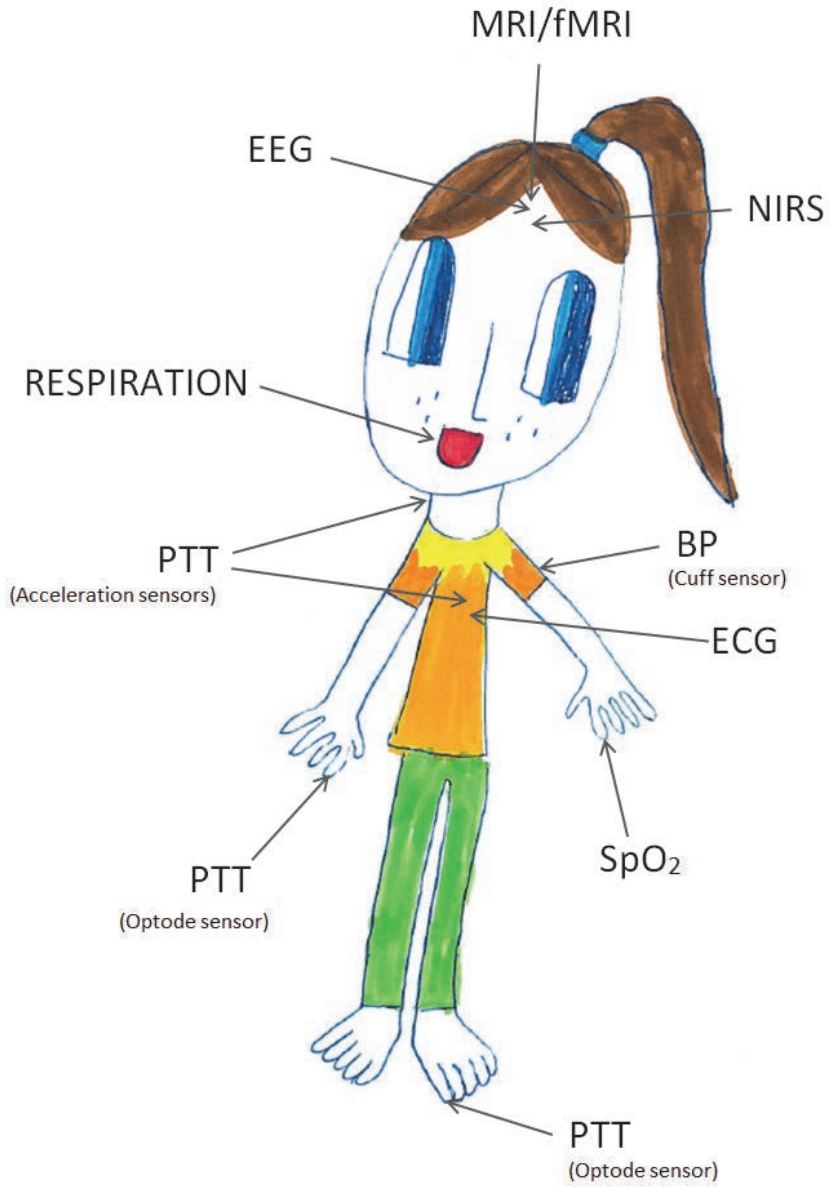


Fig. 16. Placement of sensors. Picture drawn by Auri Myllylä and coloured by Anna Myllylä.



Fig. 17. Sensor assembly. Multimodal measurements can start. On the left, measurements are conducted at the Oulu University Hospital (Finland), and on the right, in the Leibniz Institute for Neurobiology in Magdeburg (Germany). In both cases the imaging is done by 3 T closed MRI scanner, manufactured by Siemens.

For fMRI, the multimodal setup utilizes a novel ultrafast imaging technique, MREG, capable of providing a sampling rate approximately 20 - 25 times faster (10 to 16 Hz) than commonly used MRI sequences (Zahneisen *et al.*, 2012; Assländer *et al.* 2013; Testud 2013). This enables unaliased sampling of BOLD signals to study brain functions. Presenting of the multimodal data analysis method for the recorded data is not included in this thesis. However, the data analysis method for the recorded multimodal data will be described in an upcoming paper: “Synchronous multi-scale neuroimaging environment for critically sampled physiological analysis of brain function - a Hepta-scan concept”. Moreover, Paper (VI) shows results of measurements already gathered with the presented multimodal setup.

4 Results to validate the methods

Results shown in this section serve to validate the measurement methods presented in the thesis and help to estimate the reliability of the gathered data. Since ensuring the MRI compatibility of the developed devices is a highly important consideration, many of the measurements center on the issue. Papers (I, II, III) include results related to MRI-compatibility studies.

Results presented in Papers (II and VII) relate to the application of the developed NIRS device to fNIRS measurements of the brain and explore light attenuation at selected wavelengths as a function of source-detector distance. Furthermore, Paper (VII) provides results for determining light propagation in tissue and discusses the sensing depth in brain tissue achieved with the device. Most importantly, these studies strive to ensure that the optical power of LEDs is sufficiently high to allow their application to brain studies.

Paper (IV), in turn, deals with the accuracy of the responses of acceleration and optical probe (optode) sensors in determining PTT. Additionally, Paper (V) describes a case study of ECG signals, using the QRS complex as a reference in PTT measurements and explores the accuracy achievable by the presented method.

4.1 MRI compatibility of the measurement methods

MRI-compatibility studies were performed in three different MRI rooms housing the following MRI scanners:

- a) 0.23 T open C-shaped MRI scanner, manufactured by Philips Medical Systems
- b) 1.5 T closed MRI scanner, manufactured by GE
- c) 3 T closed MRI scanner, manufactured by Siemens

The measurements in (I) show that electromagnetic interference (EMI) produced by the MRI scanner is rather significant and occurs in a very wide frequency range. This has to be taken into account in the design of electrical devices to be used inside the MRI room, particularly in data transfer. Fig. 4 shows the EMI spectrum between ~ 0 Hz and 1.5 GHz generated by an MRI scanner with a vertical magnetic field of 0.23 T. It can be seen that, at 2.4 GHz, there is a narrow peak, generated in this case by a Bluetooth transceiver. Other than that, only background noise is present above 1.5 GHz, making it a fully free operating band

for transceivers. Moreover, the results in (I) revealed that electromagnetic signals produced by the radio modules under test do not affect MR imaging, provided that they are located outside the scanning volume of the MRI scanner. Fig. 18 shows how an MRI reference image became disturbed, when a wireless transceiver was located within the scanning volume. When the device was located at a distance of approximately 2 m from the centre of the scanning volume, the image was not disturbed, as shown by Fig. 19.

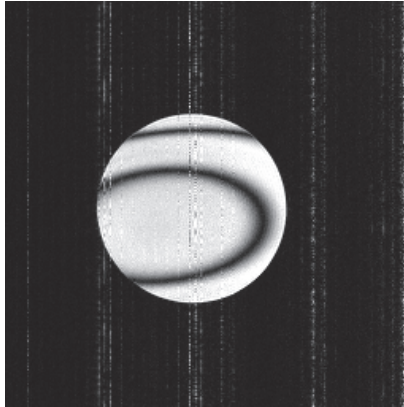


Fig. 18. Transceiver located in the scanning volume causes serious artifacts and distortions. (Paper I, published with the permission of © 2007 by University of Oulu).

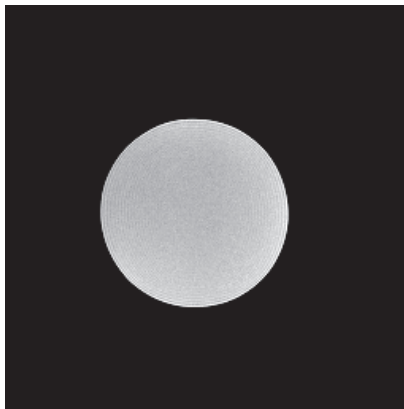


Fig. 19. MRI reference image was undisturbed, when the devices were located outside the red zone marked on the floor of the MRI room, at a distance of approximately 2 m from the 0.23T open C-shaped MRI scanner. (Paper I, published with the permission of © 2007 by University of Oulu).

Also the MR-compatibility of NIBP and NIRS devices was studied during the work leading up to this thesis. Several compatibility test measurements verified that the acceleration sensor of the NIBP system did not disturb MR images. However, it appeared that NIRS devices do disturb MR images under certain conditions, as can be seen in Fig. 20. Although the observed disturbance was low when the device was properly shielded, it was decided to place the device itself outside the MRI room and to use only its optical parts inside the room. In this way, MR compatibility could be ensured in every case. Moreover, usage of the device became easier, as it could be controlled from outside the MRI room during the entire measurement.

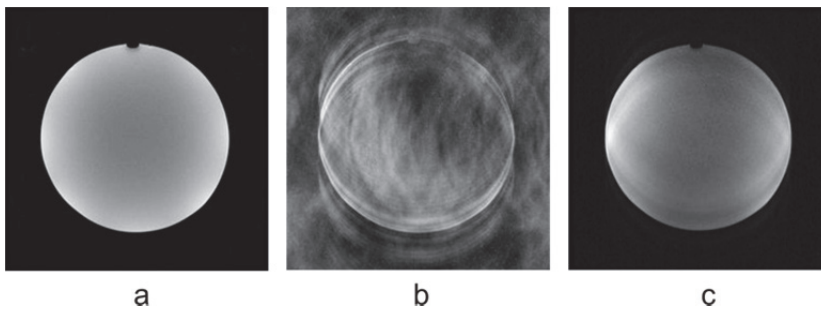


Fig. 20. MR images of a calibration phantom: (a) undisturbed reference MR image, (b) disturbed MR image obtained during unshielded 10-channel LED driver operation, and (c) slightly disturbed MR image, obtained during shielded 10-channel LED driver operation. (Paper II, published with the permission of © 2010 Turpion-Moscow Ltd).

In 2014, measurements with NIBP and NIRS devices were done also in Magdeburg, in Leibniz Institute for Neurobiology. The institute facilitates a similar kind of 3T MRI scanner by Siemens as described in c). Also these measurements, using the same setup, showed no problems with MRI compatibility.

4.2 Sensing by the NIRS device

Attenuation of modulated light was extensively studied for several reasons. Firstly, to optimize the sensitivity of the NIRS device and, secondly, to ensure that the light power generated by LEDs is high enough for sensing the cerebral cortex of the brain, and, thirdly, that the receiver and amplifier can provide sufficient

SNR. Figs. 21 and 22 show attenuation of backscattered light at different source-detector distances for wavelengths of 830 nm and 905 nm.

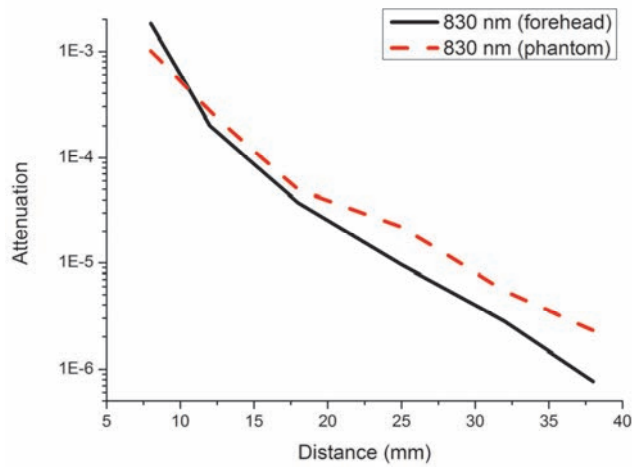


Fig. 21. Attenuation of back-scattered light at different source-detector distances on the human forehead (*in vivo*) at the wavelength of 830 nm. (Paper VII, published with the permission of © 2013 OSA-SPIE).

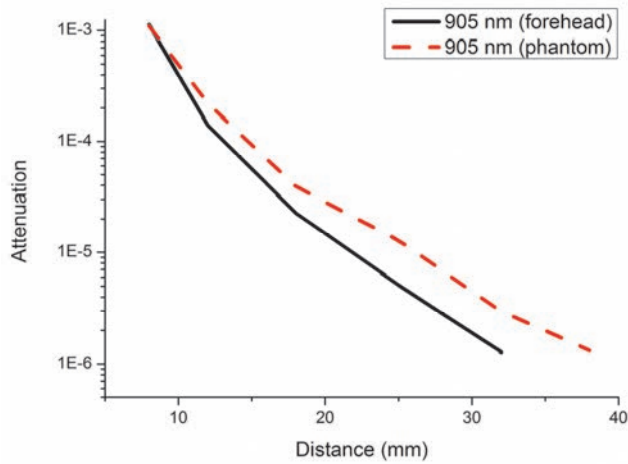


Fig. 22. Attenuation of backscattered light at different source-detector distances at the wavelength of 905 nm. (Paper VII, published with the permission of © 2013 OSA-SPIE).

One important consideration centered on estimating the highest achievable sensing depth in the head using the developed NIRS device. This was done by utilizing multi-layered optical phantoms (Bykov *et al.* 2011, Korhonen *et al.* 2014). In these measurements, light was transmitted into a forehead-mimicking phantom and the detector was placed at different distances from the light source. It is a generally accepted concept that by increasing the source-detector distance, the majority of photons travel deeper into tissue before reaching the detector, leading to an increase in sensing depth. This phenomenon is related to commonly known estimations of light propagation through a substance, where the trajectory of the photon path from source to detector is assumed to be banana-shaped in form (Zee *et al.* 1990, Okada *et al.* 1997, Cui *et al.* 2011). The test setup enables the study of this phenomenon.

In the measurement setup, PPG and NIRS fibre optic sensors are used to simultaneously sense a pulsating liquid flowing inside a silicon tube. PPG is used as reference modality, being able to sense liquid flow directly on the tube's surface. In this paper (VII), the NIRS sensor, depicted in Fig 23, refers to a sensor placed on the phantom surface at a long source-detector distance, while the PPG sensor has a source-detector distance of 5 mm. A silicon tube with a diameter of 4 mm was placed between the grey and white matter layers to determine experimentally whether the NIRS sensor is able to sense liquid movement within the tube. The general idea is to simulate a large, albeit simplified, blood vessel in the brain. Naturally, the tube can also be placed between other layers and at different horizontal positions in a layer to estimate light propagation more extensively. Particular emphasis was placed on establishing whether the device has the capability to sense movements in the grey matter of the brain at a depth of approximately 20 mm.

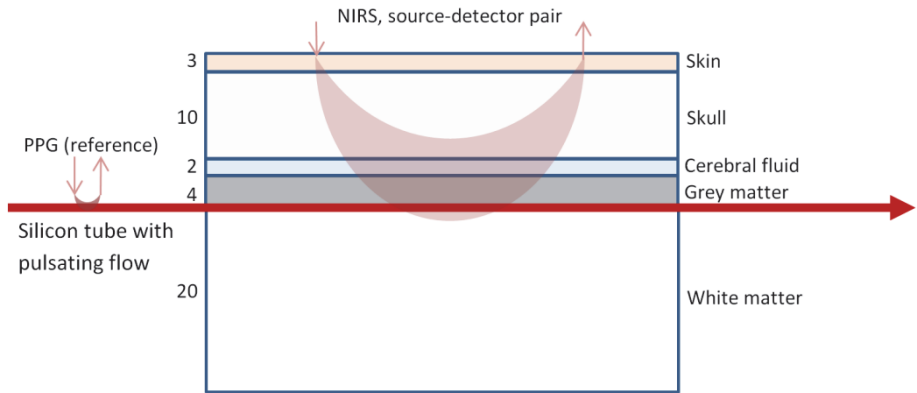


Fig. 23. NIR light illustration, with back-scattering in a banana-shaped form, reaching the tube behind the grey matter layer. The numbers represent the thickness of each layer in mm. (Paper VII, published with the permission of © 2013 OSA-SPIE).

The results of the phantom measurements indicate that the developed NIRS device has the ability to sense grey matter, if the source-detector distance is more than 3 cm and near-infra red light is used for illumination. Fig 24 shows responses of liquid pulsations measured from the tube at a source-detector distance of 4 cm, using the wavelengths of 830 nm and 905 nm.

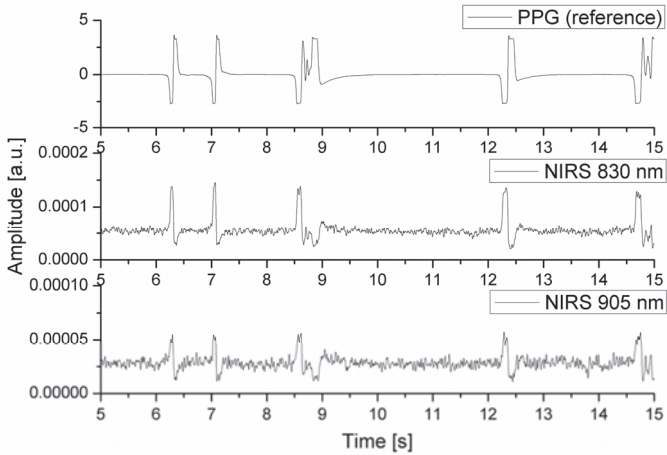


Fig. 24. NIRS responses at a source-detector distance of 4 cm. In this case, pulsations behind the grey matter layer (through skin, skull and cerebral fluid) could be sensed at the wavelengths of 830 nm and 905 nm. (Paper VII, published with the permission of © 2013 OSA-SPIE).

It must be noted that our test setup only allows sensing movement inside the tube. Thus, we could only estimate the achieved light penetration depth. This setup cannot mimic pulsating blood flow, which requires taking account of changes in blood volume and oxygenation of blood in micro vessels.

Another strand of research focused on *in vivo* measurements to determine how an increase in source-detector distance affects the dynamic response of the received signal, by analysing its spectrum. It turned out that, especially low frequency oscillations (LFOs) of cerebral hemodynamics seem to be more visible in the spectrum, when the distance between the source and the detector is 3 cm or more in the frequency range of 0,01 - 0,15 Hz (Obrig *et al.* 2000, Tong & Frederic 2010, Sasai *et al.* 2012, Korhonen *et al.* 2014). This indicates that the separation distance has to exceed 3 cm to enable sensing of cerebral hemodynamics.

4.3 HR and BP pulsation measurements

Because the slew factor of the sensor is an important factor in the PTT method, we studied the transient responses of our accelerometer sensor to generated mechanical impulses. In this experiment, a mechanical pulse was focused on the sensor surface by touching the acceleration sensor with an object made of a current-conducting material with a constant voltage level. Moreover, for test purposes, the surface of the accelerometer was covered with a thin copper tape that was grounded. The idea in this arrangement was that the moment the object touches the accelerometer, its voltage drops, because it is now in contact with a grounded surface. By measuring the voltage of the object during the experiment, the moment of mechanical impulse on the surface can be accurately determined. As indicated by Fig. 25, vibrations start instantly (with a delay of less than 1ms) as the object touches the sensor surface. After contact, the vibrations begin to attenuate almost linearly.

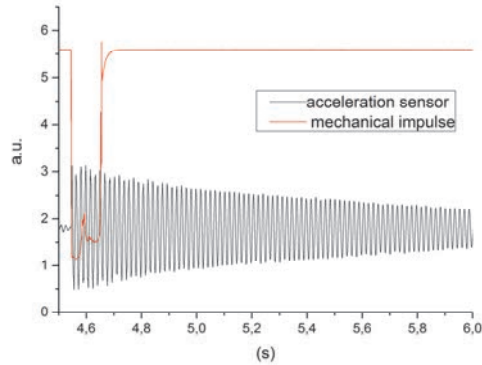


Fig. 25. Transient showing the slew rate of the acceleration sensor. A sensor with a grounded surface was touched by a current contacting object, having a voltage level of 5.6 V. The moment of contact is visible as a voltage drop in the object (red curve), which thus determines the time point of contact. As can be seen, the acceleration sensor reacts very fast to an impulse, while requiring a long relaxation time. This measurement used a sampling rate of 50 kHz.

As already mentioned, an accurate time-domain determination of heart pulse waves by sensors allows calculating PTT between different sensors. In addition, PTT between ECG and the sensors can be determined, because our setup measures ECG signals during MRI. The R wave of the QRS complex of ECG is used in determining PTT values during continuous non-invasive monitoring of BP (V). However, standard electrode placement cannot be used in the MRI environment, lest they disturb imaging. As a result, electrode placement in the MRI room can vary widely between measurements.

With different electrode placements, determining the time resolution of an ECG sensor hinges on the QRS time point of ECG and the shape of the QRS complex. Our results show that the position of the R peak in the time axis varies depending on electrode placement. Fig. 26 shows an example of a simultaneous measurement of ECG using two different electrode placements. These two configurations, employing three electrodes, differ only in that in the first one, called ECG (back), the (-) electrode is placed on the back, while in the other configuration, called ECG (normal), the (-) electrode is located on the chest. The remaining two electrodes, (+) and ref, were in the same position in both measurements. In this case, the difference in the placement of the (-) electrode caused a difference of 10ms between the R peaks in the time axis. In general, different placements on the chest caused a time change of a few milliseconds for

the R wave. This must be considered when R wave of ECG is used in determining PTT during MRI.

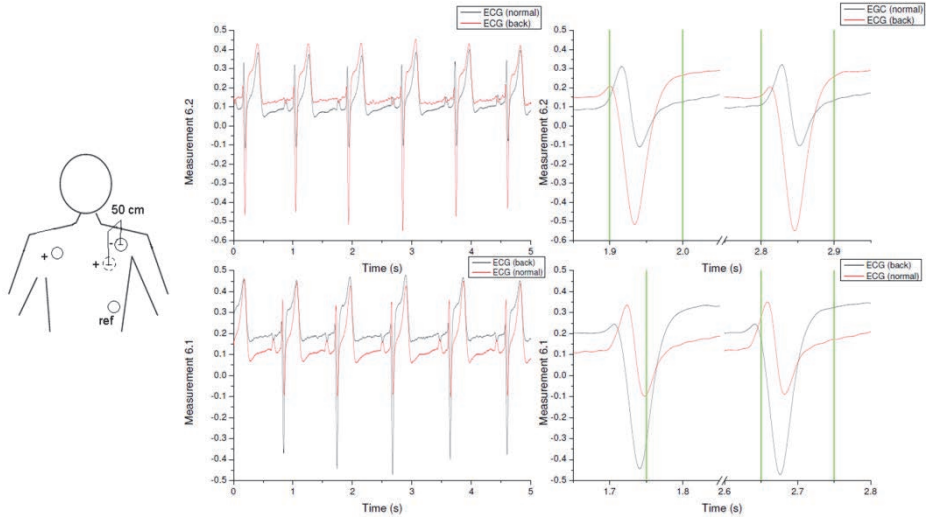


Fig. 26. Measurements 6.1 and 6.2. The replaced (+) electrode was located on the back and the distance between the (+) and (-) electrodes was 50cm. This caused a delay of approx. 10ms in the R wave, highlighted on the right showing one R wave. (Paper V, published with the permission of © 2013 SPIE).

Fig. 27 and 28 show how PTT follows the change of BP measured by cuff occlusion, at a time interval of 60 seconds. In this example, for better illustration, PTT values between ECG and PPG are only taken from the moment the cuff was measuring, although PTT can be determined for each heart pulse.

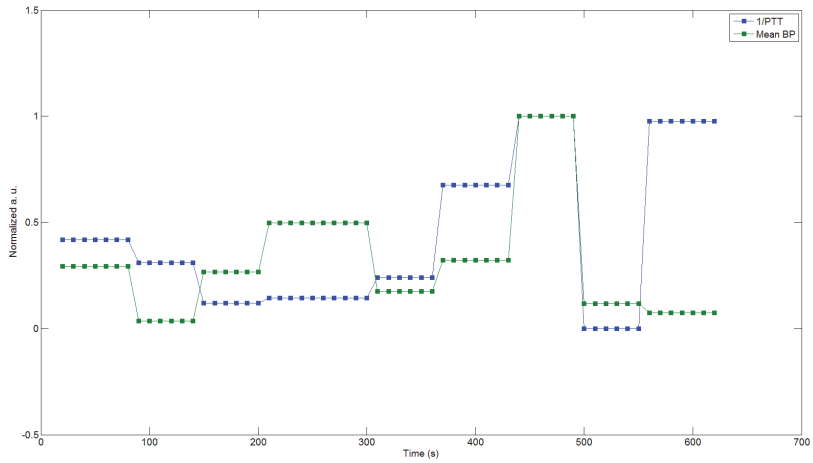


Fig. 27. Comparison between 1/PTT signals, measured by acceleration sensors placed on the chest and in the neck, and BP measured by a cuff, placed on the left arm. The measurement was taken during MRI.

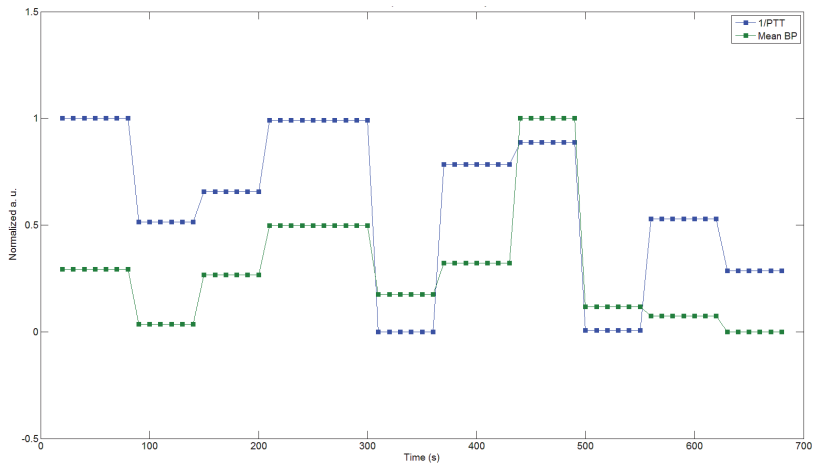


Fig. 28. Comparison of BP to 1/PTT signals, measured between ECG and PPG, when PPG is placed on a finger in the same arm where the cuff is placed. The measurement was taken during MRI.

The responses, shown in Figs. 27 and 28, indicate that there is a correlation between PTT and BP measured by cuff. It is notable that 1/PTT follows changes in BP better in Fig. 27 than in Fig. 28. A probable reason is that, in Fig. 28, PTT

and BP are measured from the same arm, whereas in Fig. 27, PTT is measured between the chest and the neck, where BP can be different than in the arm.

We had recently an opportunity to measure BP during a clinical operation on an anaesthetized patient using a continuous invasive blood pressure (IBP) method and our multimodal setup. Fig. 29 shows BP responses acquired by an invasive BP measurement and the NIBP measurement with accelerometers. As this example illustrates, results obtained with the accelerometer-based NIBP measurement correspond well to the upper envelope of IBP.

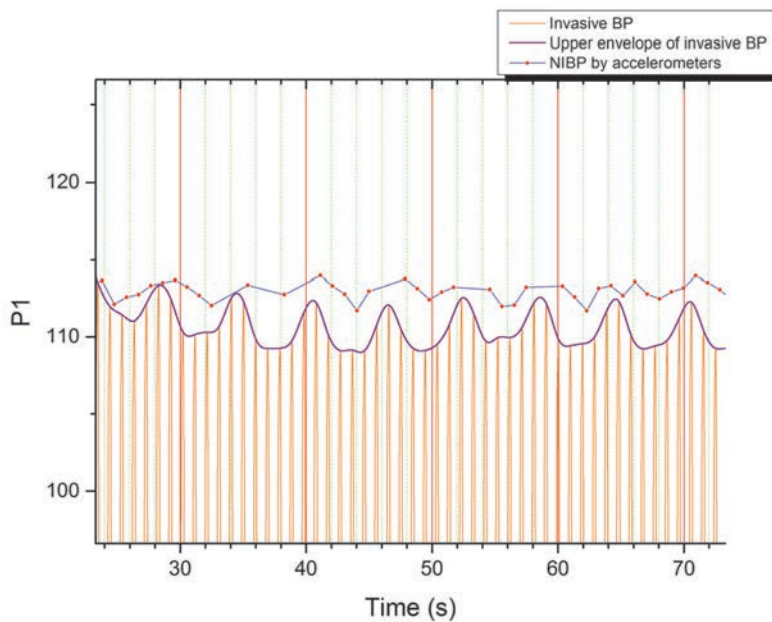


Fig. 29. Simultaneous measurement of BP by the developed NIBP method and by an anaesthesia monitoring device, GE Datex-Ohmeda, measuring BP invasively. The sampling rate of NIBP measurement was 1 kHz and that of the anaesthesia monitoring device 400 kHz.

Fig. 30 presents an example of responses obtained by fibre optical sensors and ECG (IV). As seen, the developed sensors are capable of sensing HR and pulsations generated by BP extensively and accurately from the human body during MRI scanning. Thus, their signal response accuracy is sufficient for determining PTT values.

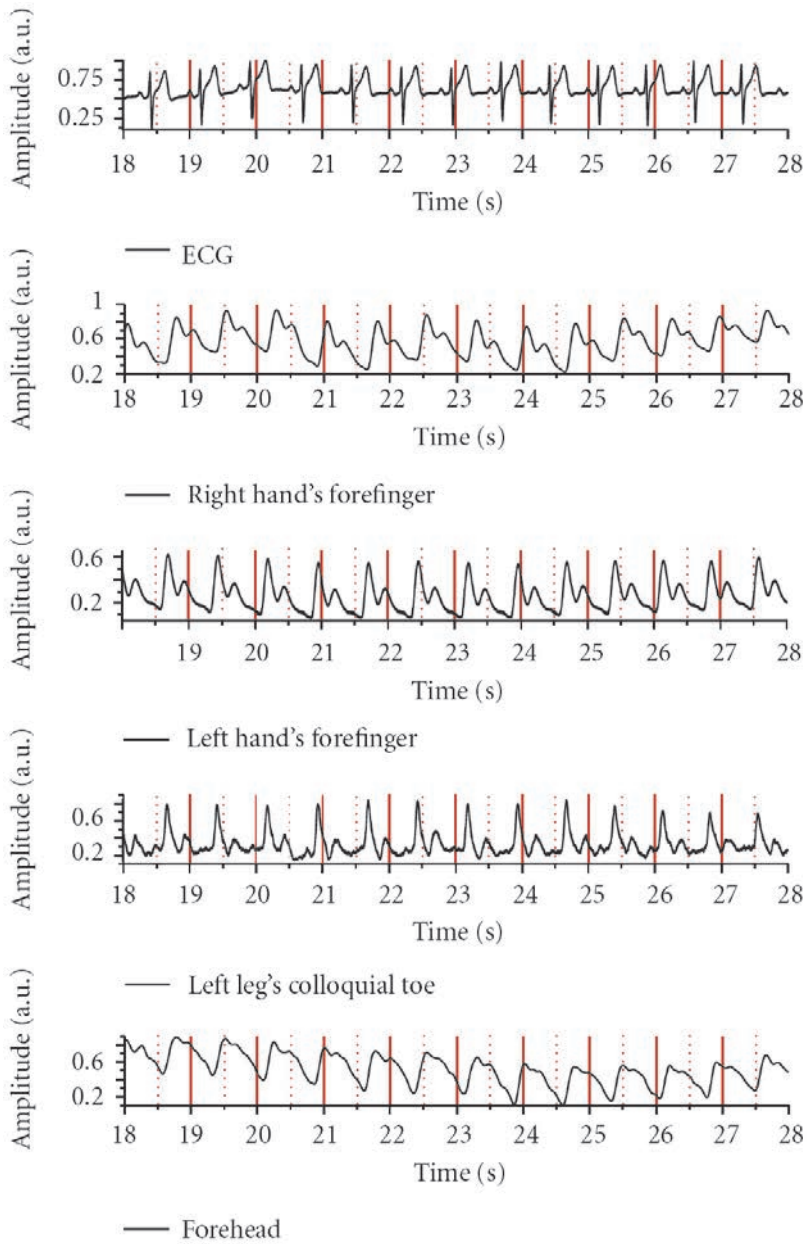


Fig. 30. Measurement 1: ECG and blood flow pulsation responses using optode sensors in different parts of the human body. (Paper IV, published with the permission of © 2012 by Hindawi Publishing Corporation).

4.4 Synchronised response of different pulsations during MRI

Fig. 31 depicts a typical response acquired in a simultaneous measurement using the developed devices. This measurement, conducted in the MRI room, proceeded for 100 seconds. Placed on the chest and neck, NIBP acceleration sensors showed vibrations as a function of heart pulses. In this figure, wavelengths used during NIRS are marked 1–3, corresponding to 660 nm, 830 nm and 905 nm, respectively, and the NIRS sensor was placed on the forehead. Values for Deoxy and Oxy are calculated at the wavelengths of 660 nm and 830 nm. Although the ECG signal was disturbed in most cases, it is possible to trace the R wave to calculate HR and to obtain PTT.

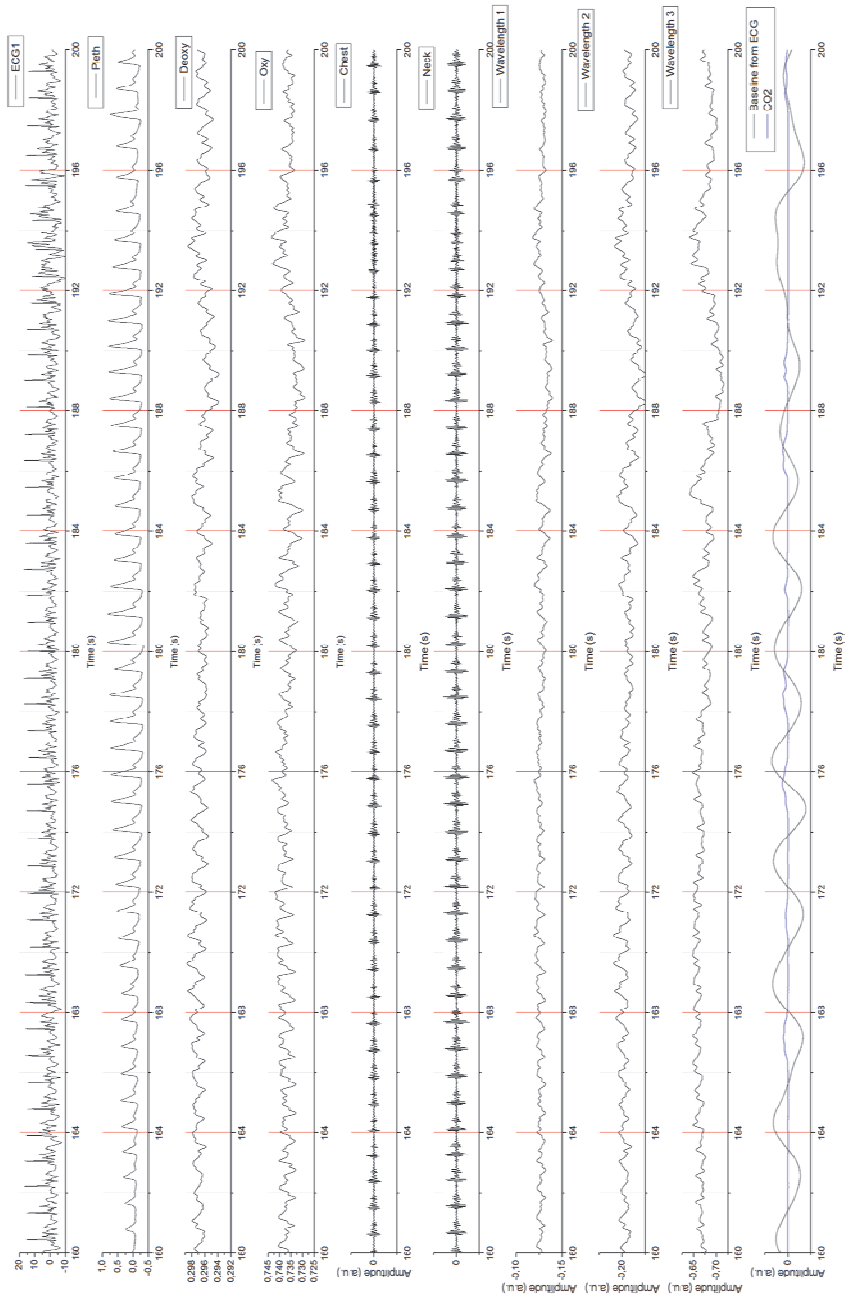


Fig. 31. Dynamics of the human body measured simultaneously by different sensors.

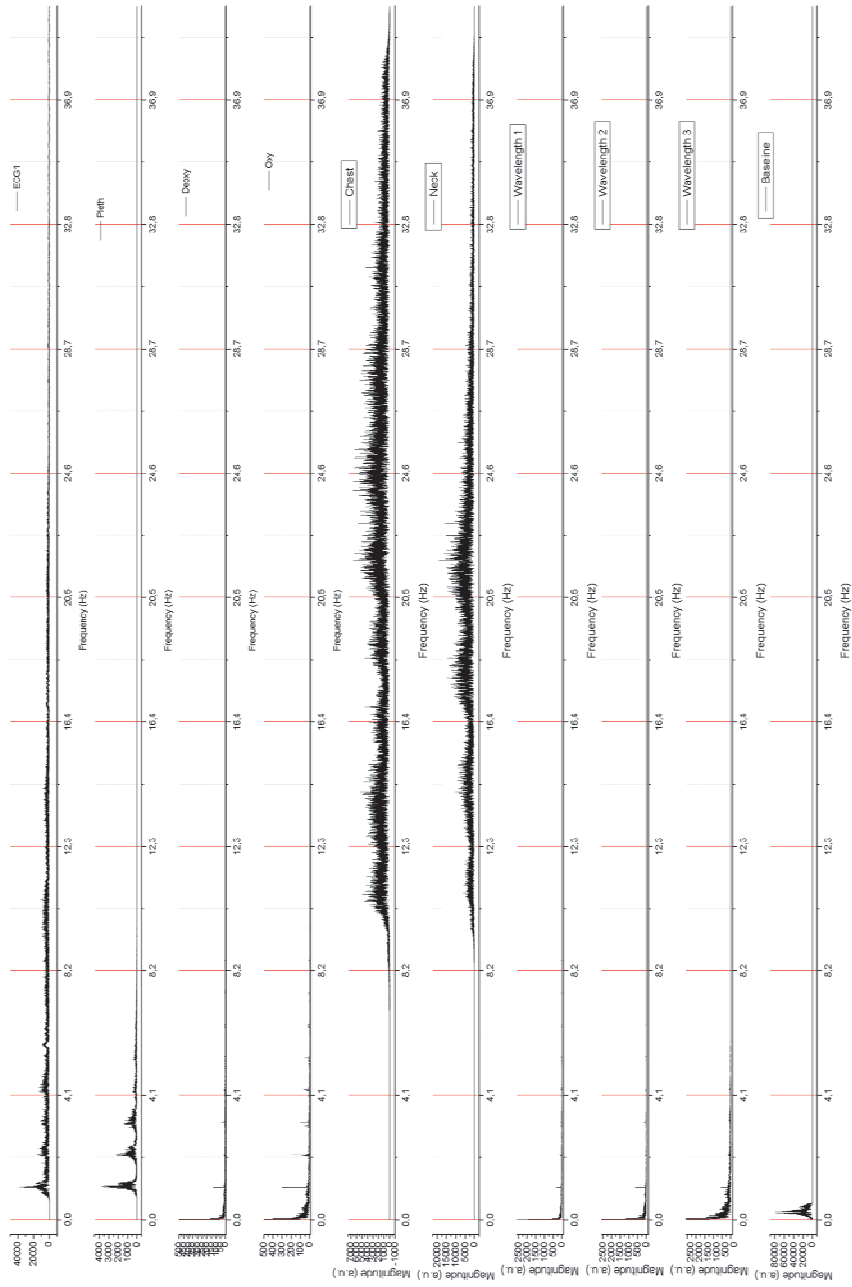


Fig. 32. Corresponding spectra for the responses shown in Fig. 31.

Fig. 32 shows the corresponding spectra for the responses in Fig. 31. Interestingly, it appears that the different sensors record physiological dynamics in different spectral ranges, depending largely on the sensing technique, but also on different positioning of sensors on the body. NIBP acceleration sensors in particular show that mechanical vibrations, caused by BP pulses, exist mainly in the frequency range of 10 Hz to 35 Hz, which is below the resonance frequency mentioned earlier in Fig 14.

5 Discussion

This section deals with some separate issues related to the measurement methods, particularly their limitations and planned improvements. Finally, current and future work with the multimodal setup will be discussed.

5.1 Limitations and possible improvements

5.1.1 Spatial resolution of NIRS

As already stated, probably the most notable limitation of NIRS is its limited spatial resolution. NIRS devices commonly have a spatial resolution of approximately 20 mm, when measuring deep within a tissue such as the grey matter of the brain. A useful method for improving spatial accuracy involves the use of multidetector probes (Boas *et al.* 2004), which allow measurements of back-scattered light at different distances to be combined in order to obtain scattering and absorbance properties. This is also our aim, and we are currently testing different types of detector rows, one example of which is shown in Fig. 33. Increasing the number of channels for clinical measurements also improves spatial accuracy.

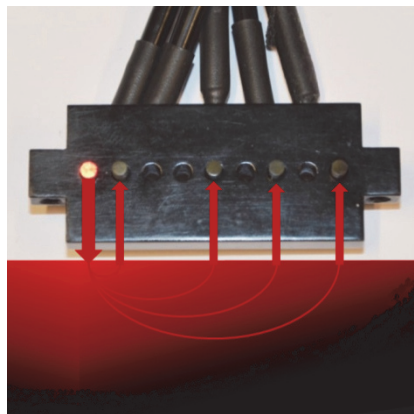


Fig. 33. Detector row and below it an illustration of light back-scattering from tissue. By placing several fibre detectors at different distances from the illuminating source, we may obtain scattering and absorbance properties with improved spatial accuracy.

Spatial resolution also depends on the anatomy of the individual brain, due to the 3D structure of multiple tissue layers. MRI enables us to build phantom models of these layer structures and to use these 3D phantoms to study light propagation (Korhonen *et al.* 2014). Further studies will be undertaken to estimate spatial resolution using this method.

When amplitude-modulated light illuminates a tissue, a phase shift (PS) occurs between the transmitted and received modulation signal. This PS is dependent on the optical path of light within the tissue before reaching the detector. The optical path length can be calculated by the equation

$$OPL = DPF \cdot d \quad (20)$$

where d is the absolute path length (distance between the source and the detector) and DPF accounts for the increased distance that light travels from the source to the detector due to scattering and absorption effects (Zee *et al.* 1992, Essenpreis *et al.* 1993, Duncan *et al.* 1995 & 1996, Boas *et al.* 2001, Strangman *et al.* 2003). Moreover, using the FD technique presented in Section 3.1.1., we may estimate the length of the optical path that light travels. In this method, modulated light from a source is sent simultaneously to the tissue under study and a reference detector. Another detector is used to record light that back-scatters from the tissue. Then, a comparison is conducted between the phase shifts of the signals received by the two detectors, and if the total PS is within one cycle, the absolute path length can be calculated as follows:

$$d = \frac{\Phi_c(c/n)}{2\pi f} \quad (21)$$

where Φ_c is the absolute phase shift, c the speed of light, n the refractive index of the tissue and f the modulation frequency (Arridge *et al.* 1992, Duncan *et al.* 1996, Peiponen *et al.* 2009). As Equation (21) indicates, a higher frequency produces a higher spatial resolution.

However, detecting a PS in a short optical path, approximately few centimetres in brain tissue (Duncan *et al.* 1995, Zee *et al.* 1992), requires a sufficiently high modulation frequency. For instance, using Equation (21), a phase shift of $0,1^\circ$ corresponds to a 2 mm difference in optical path length at the modulation frequency of 20 MHz (Castagnet *et al.* 2006). A modulation frequency of 250 kHz is near the limit of HP LEDs' capability, and at this frequency, a phase shift of $0,1^\circ$ corresponds to a path length of approximately 15

cm, which means that, in our NIRS device, the possibility of optical path length estimation in tissue using PS is limited.

Lasers or LDs do not suffer from such limitations, because they can produce much higher frequencies, as long as the modulation does not exceed the frequency of 200 MHz, as the linear relationship between PS and path length no longer applies (Arridge *et al.*, 1992).

5.1.2 R peak of the QRS complex to calculate PTT during MRI

ECG signals are normally measured with electrodes placed in accordance with standardized guidelines. This is important, because misplaced ECG electrodes can cause waveform changes, which may impact clinical decisions (McCann *et al.* 2007). In clinical measurements, however, small millisecond changes in the time delays of ECG waves are not important. In PTT measurements, though, where time delays are measured with an accuracy of milliseconds, the placement of ECG electrodes has a distinct effect on the results.

The waveform of ECG can be divided into 6 different components, known as P, Q, R, S, T and U, which reflect the process of a spreading electrical impulse in the heart. When using ECG in PTT calculations, it is customary to obtain the highest or lowest point of the R wave. Our results show that the position of the R peak in the time axis depends on electrode placement (V). Although variations in the time axis are small, they may be relevant in situations where the R wave of the ECG is used as a reference in PPT measurements of blood flow. Furthermore, when ECG is measured inside the MRI room, standardized electrode placement cannot be followed, due to interference problems caused by MRI. This increases the possibility of obtaining skewed PTT values. Consequently, when recording ECG in the MRI room to obtain PTT, special attention must be paid to using the same electrode placement in every measurement.

5.1.3 NIBP by accelerometers

Validation of NIBP measurement by accelerometers is still in progress. So far, comparisons between NIBP and IBP responses indicate a good correspondence. However, more measurements are still needed to provide a numerical evaluation of the NIBP method's accuracy and correlation to IBP. We are working on improvements to attaching sensors on the skin. Work is also in progress to enhance accuracy and reliability in situations where one sensor temporarily fails

to produce a good signal. BP must then be determined on the basis of responses provided simultaneously by more than two acceleration sensors.

5.1.4 Technical improvements of the NIRS device

SNR is dependent on several physiological signals of interest, particularly in the frequency range in which they appear. At the moment, we are interested mostly in the frequency range of 0.009–0.15 Hz. In this range, the developed NIRS device has a SNR of approximately 10 dB at the wavelength of 660 nm and a SNR of 14 dB at the wavelength of 830 nm, when comparing raw signal peaks to background noise. Naturally, it is difficult to determine exactly which peaks represent physiological signals and which can be considered as noise. In this case, we assume that physiological signals appear with regularity at specific frequencies. Determining SNR in measurements of biosignals is a complicated task, and one that we need to study in more detail in the future.

Furthermore, SNR also depends on features of the receivers. In our device, SNR is greatly dependent on the bandwidth of the filters used in the receiver, as described in Paper (II). Basically, the narrower the filter bandwidth is, the less noise we get, with a corresponding improvement in achieved SNR. Therefore, one future task we face involves improving the hardware filters of the receiver. On the other hand, narrower filters demand more stability from the modulators driving the LEDs. Additionally, to improve SNR, photodetectors with improved sensitivity are being continuously searched for, although existing detectors, with a noise-equivalent power (NEP) of 6.8×10^{-16} W/Hz^{1/2}, are sufficiently sensitive for the intended purpose, Paper (II).

Recent developments in LD technology, with an increased range of possible wavelengths and improved compactness of size, are making LDs an attractive option for our application. In comparison to LDs, the main weakness of LEDs is their limited frequency band, as described in Section 5.1.1. In addition to offering a higher frequency band, LDs also have the edge over LEDs by allowing us to improve SNR by increasing illumination power. Furthermore, it is likely that the prices of LDs will soon be comparable to those of LEDs.

5.1.5 Development of a wearable NIRS sensor

Devices for monitoring the brain are still mainly used in hospitals, but portable monitoring applications have emerged, most of them offering EEG

measurements. Some research groups have recently started developing portable fNIRS systems for brain monitoring during movement and exercise tasks outside the hospital environment (Everdell *et al.* 2013, Piper *et al.* 2014). The technique used in our NIRS device can also be implemented in a wearable version. Accordingly, this is one of our key development areas.

Consequently, in the near future, cardiac, vascular and brain functions may be continuously monitored at home using synchronized wireless equipment.

5.2 Current and future work with the multimodal setup

The goal in this work was to continuously measure metabolism, Hb and HbO₂ in particular, in the cortex, and to monitor BP fluctuations using non-invasive methods, especially during MRI. Currently, the developed multimodal system is being used on a weekly basis at the Oulu University Hospital. This strongly indicates that both goals of the thesis have been accomplished. Further, the developed multimodal system forms a foundation for multimodal studies conducted by the OFNI group, where the author is the person responsible for NIRS and NIBP. At present, the OFNI group is involved in conducting several different *in vivo* medical studies at the Oulu University Hospital. Naturally, different studies require placing special attention on the development of measurement methods and instrumentations. Hence, work to further develop multimodal measurement methods continues unabated between the OEM Laboratory and OFNI group, and with other collaborators outside the University of Oulu. The current situation is ideal for improving measurement methods, because *in vivo* measurements can be conducted with regularity, providing instant feedback and an opportunity to react rapidly to new ideas.

At the present time, the multimodal setup is utilized for instance in the study of narcolepsy and epilepsy. Moreover, we have started to develop monitoring methods, using the multimodal setup, for blood brain barrier disruption (BBBD) therapy, a treatment method for brain lymphoma. BBBD treatment allows the passage of chemotherapy drugs through the protective blood brain barrier (BBB) (Carvey *et al.* 2009) that lines the blood vessels of the brain. The BBBD procedure facilitates the delivery of drugs to a tumour and to areas of the brain around the tumour (Neuwelt 1998, Angelov *et al.* 2009).

Fig. 34 shows a computed tomography angiography (CTA) image, taken during BBBD treatment. Clearly visible in this image are NIRS and EEG sensors,

attached on the head, illustrating the positions at which the sensors are measuring physiological dynamics of the brain during treatment.

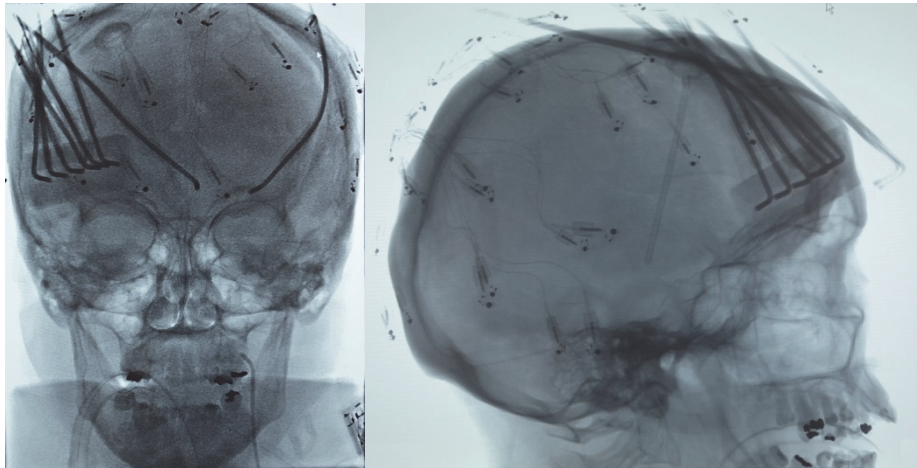


Fig. 34. CTA images of the human head taken during BBBD. Optical fibres for NIRS and electrodes for EEG are clearly visible.

Lastly, it must be emphasized that simultaneous measurement of so many modalities requires good planning and organization among involved personnel. As individuals within the group represent different educational backgrounds, specific attention must be given to communication among them. The design and construction of the multimodal setup draws on a combination of skills acquired by persons with a background in physics, medicine and engineering. At the same time, the work reported here gives the participants an opportunity to obtain and take back valuable information to their separate professional fields. In a sense, biomedical engineering and physics provide tools and help to build a basis for medical research. That is what I call functional multimodal biomedical research.

6 Conclusion

The presented methods allow simultaneous continuous measurement of HR and metabolism in the cortex as well as PWV and BP measurements in synchrony with EEG and MRI. Furthermore, the thesis explored the reliability and accuracy of the responses gathered by the developed instruments and presents a multimodal measurement setup for medical studies.

References

- Alderliesten T, De Vis JB, Lemmers PMA, van Bel F, Benders MJNL, Hendrikse J & Petersen ET (2014) Simultaneous quantitative assessment of cerebral physiology using respiratory-calibrated MRI and near-infrared spectroscopy in healthy adults. *Neuroimage* 85: 255–263.
- Allen J (2007) Photoplethysmography and its application in clinical physiological measurement. *Physiol Meas* 28(3): R1.
- Angelov L, Doolittle ND, Kraemer DF, Siegal T, Barnett GH, Peereboom DM, Stevens G, McGregor J, Jahnke K, Lacy CA, Hedrick NA, Shalom E, Ference S, Bell S, Sorenson L, Tyson RM, Haluska M & Neuwelt EA (2009) Blood-brain barrier disruption and intra-arterial methotrexate-based therapy for newly diagnosed primary CNS lymphoma: a multi-institutional experience. *J Clin Oncol* 27(21): 3503–9. DOI: 10.1200/JCO.2008.19.3789.
- Arridge SR, Cope M & Delpy DT (1992) Theoretical basis for the determination of optical pathlengths in tissue: temporal and frequency analysis. *Phys Med Biol* 37:1531–1560.
- Aszländer J, Zahneisen B, Hugger T, Reiser M, Lee H, LeVan P & Hennig J (2013) Single shot whole brain imaging using spherical stack of spirals trajectories. *Neuroimage* 73: 59–70.
- ASTM International (2005) American Society for Testing and Materials (ASTM) International, Designation: F2503-05. Standard Practice for Marking Medical Devices and Other Items for Safety in the Magnetic Resonance Environment.
- Bakker A, Smith B, Ainslie P & Smith K (2012) Near-Infrared Spectroscopy, Applied Aspects of Ultrasonography in Humans. In Ainslie P (ed) *Applied Aspects of Ultrasonography in Humans*. ISBN: 978-953-51-0522-0.
- Berger H (1929) Über das Elektroencephalogramm des Menschen. *Archiv für Psychiatrie und Nervenkrankheiten* 87(1): 527–570.
- Biswal B, Yetkin FZ, Haughton VM & Hyde JS (1995) Functional connectivity in the motor cortex of resting human brain using echo-planar MRI. *Magn Reson Med* 34(4): 537–541.
- Boas DA, Gaudette T, Strangman G, Cheng X, Marota JJA & Mandeville JB (2001) The Accuracy of Near Infrared Spectroscopy and Imaging during Focal Changes in Cerebral Hemodynamics. *NeuroImage* 13: 76–90.
- Boas DA, Chen K, Grebert D & Franceschini MA (2004) Improving the diffuse optical imaging spatial resolution of the cerebral hemodynamic response to brain activation in humans. *Opt Lett* 29: 1506–1508.
- Bykov AV, Popov AP, Priezzhev AV & Myllylä RA (2011) Multilayer tissue phantoms with embedded capillary system for OCT and DOCT imaging. *Proc SPIE vol. 8091: 80911R-1–80911R-6*.
- Cao Q, Zhegalova N, Wang S, Akers W & Berezin M (2013) Multispectral imaging in the extended near-infrared window based on endogenous chromophores. *Journal of Biomedical Optics* 18(10): 1013–1018.
- Carmen-Gabriela S (2012) *Magnetism Basics and Applications*, XXIV.

- Carvey PM, Hendey B & Monahan AJ (2009) The blood-brain barrier in neurodegenerative disease: a rhetorical perspective. *J Neurochem* 111(2): 291–314. DOI: 10.1111/j.1471-4159.2009.06319.x.
- Castagnet D, Tap-Béteille H & Lescure M (2006) Avalanche-photodiode-based heterodyne optical head of phase-shift laser ranger finder. *Opt Eng* 45: 04003-1–043003-7.
- Cooper CE, Cope M, Quaresima V, Ferrari M, Nemoto E, Springett R, Matcher S, Amess P, Penrice J, Tyszczyk L, Wyatt J & Delpy DT (1997) Measurement of Cytochrome Oxidase Redox State by Near Infrared Spectroscopy. *Adv Exp Med Biol* 413: 63–73.
- Cooper CE, Cope M, Springett R, Amess PN, Penrice J, Tyszczyk L, Punwani S, Ordidge R, Wyatt J & Delpy DT (1999) Use of Mitochondrial Inhibitors to Demonstrate That Cytochrome Oxidase Near-Infrared Spectroscopy Can Measure Mitochondrial Dysfunction Noninvasively in the Brain. *J Cereb Blood Flow Metab* 19(1): 27–38.
- Cope M & Delpy D (1988) System for long-term measurement of cerebral blood and tissue oxygenation on newborn infants by near infra-red transillumination. *Medical and Biological Engineering and Computing* 26(3): 289–294.
- Cope M (1991) The application of near infrared spectroscopy to non-invasive monitoring of cerebral oxygenation in the newborn infant. *Department of Medical Physics and Bioengineering*: 342.
- Cope M, van der Zee P, Essenpreis M, Arridge SR & Delpy DT (1991) Data analysis methods for near infrared spectroscopy of tissue: Problems in determining the relative cytochrome aa3 concentration. *SPIE* 1431: 251–262.
- Cui X, Bray S, Bryant DM, Glover GH & Reiss AL (2011) A quantitative comparison of NIRS and fMRI across multiple cognitive tasks. *Neuroimage* 54(4): 2808–2821.
- Delpy DT, Cope M, van der Zee P, Arridge S, Wray S & Wyatt J (1988) Estimation of optical pathlength through tissue from direct time of flight measurement. *Phys Med Biol* 33 (12): 1433–1442.
- Duan L, Zhang Y & Zhu C (2012) Quantitative comparison of resting-state functional connectivity derived from fNIRS and fMRI: A simultaneous recording study. *Neuroimage* 60(4): 2008–2018.
- Duncan A, Meek JH, Clemence M, Elwell CE, Tyszczyk L, Cope M & Delpy DT (1995) Optical pathlength measurements on adult head, calf and forearm and the head of the newborn infant using phase resolved optical spectroscopy. *Phys Med Biol* 40: 295–304.
- Duncan A, Meek JH, Clemence M, Elwell CE, Fallon P, Tyszczyk L, Cope M & Delpy DT (1996) Measurement of Cranial Optical Path Length as a Function of Age Using Phase Resolved Near Infrared Spectroscopy. *Pediatric Research* 39: 889–894.
- Dyer R (2006) Magnetic resonance imaging compatibility and safety of the SOUNDTEC Direct System. *Laryngoscope* 116(8): 1321–1333.
- Essenpreis M, Elwell CE, Cope M, van der Zee P, Arridge SR & Delpy DT (1993) Spectral dependence of temporal point spread functions in human tissues. *Applied Optics* 32: 418–425.
- ETS Lingren (2009) MRI shielding architectural site planning guide.

- Everdell NL, Airantzis D, Kolvyta C, Suzuki T & Elwell CE (2013) A portable wireless near-infrared spatially resolved spectroscopy system for use on brain and muscle. *Med Eng Phys* 35(11): 1692–1697.
- Expert Panel on MR Safety:, Kanal E, Barkovich AJ, Bell C, Borgstede JP, Bradley WG, Froelich JW, Gimbel JR, Gosbee JW, Kuhni-Kaminski E, Larson PA, Lester JW, Nyenhuis J, Schaefer DJ, Sebek EA, Weinreb J, Wilkoff BL, Woods TO, Lucey L & Hernandez D (2013) ACR guidance document on MR safe practices: 2013. *Journal of Magnetic Resonance Imaging* 37(3): 501–530.
- Ferrari M & Quaresima V (2012) A brief review on the history of human functional near-infrared spectroscopy (fNIRS) development and fields of application. *NeuroImage*. DOI: 10.1016/j.neuroimage.2012.03.049.
- Ferrari M, Mottola L & Quaresima V (2004) Principles, techniques, and limitations of near infrared spectroscopy. *Can J Appl Physiol* 29(4): 463–487.
- Gesche H, Grosskurth D, Kuchler G & Patzak A (2012) Continuous blood pressure measurement by using the pulse transit time: Comparison to a cuff-based method. *Eur J Appl Physiol*. 112: 309–315.
- Gribbin B, Steptoe A & Sleight P (1976) Pulse Wave Velocity as a Measure of Blood Pressure Change. *Psychophysiology* 13(1): 86–90.
- Hahn R, Rinösl H, Neuner M & Kettner SC (2012) Clinical validation of a continuous non-invasive haemodynamic monitor (CNAP™ 500) during general anaesthesia. *Br J Anaesth* 108: 581–585.
- Hakim KA (2011) Continuous non-invasive BP monitoring; service evaluation during induction of anaesthesia and haemodialysis. Dr Thesis.
- Hast J (2003) Self-mixing interferometry and its applications in noninvasive pulse detection. *Acta Univ Oul C* 182.
- Hoge RD, Franceschini MA, Covolan RJM, Huppert T, Mandeville J B & Boas DA (2005) Simultaneous recording of task-induced changes in blood oxygenation, volume, and flow using diffuse optical imaging and arterial spin labeling MRI. *Neuroimage* 25: 701–707.
- Hugger T, Zahneisen B, LeVan P, Lee KJ, Lee H-L, *et al.* (2011) Fast Undersampled Functional Magnetic Resonance Imaging Using Nonlinear Regularized Parallel Image Reconstruction. *PLoS ONE* 6(12): e28822. DOI:10.1371/journal.pone.0028822.
- Huppert TJ, Hoge RD, Diamond SG, Franceschini MA & Boas DA (2006) A temporal comparison of BOLD, ASL, and NIRS hemodynamic responses to motor stimuli in adult humans. *Neuroimage* 29(2): 368–382.
- Indic P, Salisbury EB, Paydarfar D, Brown EN & Barbieri R (2008) Interaction between heart rate variability and respiration in preterm infants. *Computers in Cardiology*: 57–60.
- Ishikawa D (2014) Recent progress of near-infrared (NIR) imaging--development of novel instruments and their applicability for practical situations. *The international journal of the Japan Society for Analytical Chemistry*.
- Jenkins J & Gerred S (2009) A brief history of electrocardiography. URI: <http://www.ecglibrary.com/ecghist.html>.

- Jöbsis FF (1977) Non invasive, infrared monitoring of cerebral and myocardial oxygen sufficiency and circulatory parameters. *Science* 198: 1264–1267.
- Kerola J, Kontra V & Sepponen R (1996) Non-invasive blood pressure data acquisition employing pulse transit time detection. *Engineering in Medicine and Biology Society, 1996. Bridging Disciplines for Biomedicine. Proceedings of the 18th Annual International Conference of the IEEE* 3: 1308–1309.
- Kiviniemi V (2008) Endogenous brain fluctuations and diagnostic imaging. *Hum Brain Mapp* 29(7): 810–817.
- Korhonen VO, Myllylä TS, Kirillin MY, Popov AP, Bykov AV, Gorshkov AV, Sergeeva EA, Kinnunen M & Kiviniemi V (2014) Light Propagation in NIR Spectroscopy of the Human Brain. *IEEE Journal of Selected Topics in Quantum Electronics* 20(2): 289–298.
- Kroll RA & Neuwelt EA (1998) Outwitting the blood-brain barrier for therapeutic purposes: osmotic opening and other means. *Neurosurgery* 42: 1083–1099. Discussion 1099–1100.
- Kurth CD & Thayer WS (1999) A multiwavelength frequency-domain near-infrared cerebral oximeter. *Phys Med Biol* 44(3): 727.
- Lass J, Meigas K, Karai D, Kattai R, Kaik J & Rossmann M (2004) Continuous blood pressure monitoring during exercise using pulse wave transit time measurement. *Engineering in Medicine and Biology Society, 2004. IEMBS '04. 26th Annual International Conference of the IEEE* 1: 2239–2242.
- Lesage F, Bonnery C & Pouliot P (2013) *Diffuse Optical Tomography and Biophysical Modeling of the Aging Brain*. Berlin Heidelberg, Springer.
- Madsen SJ (ed) (2013) *Optical Methods and Instrumentation in Brain Imaging and Therapy*. New York, Springer.
- Marcinkevics Z, Greve M, Aivars JI, Erts R & Zehtabi AH (2009) Relationship between arterial pressure and pulse wave velocity using photoplethysmography during the post-exercise recovery period. *Acta Universitatis Latviensis: Biology* 753: 59–68.
- Marinkovic K, Baldwin S, Courtney M, Witzel T, Dale A & Halgren E (2011) Right hemisphere has the last laugh: neural dynamics of joke appreciation. *Cognitive, Affective, & Behavioral Neuroscience* 11(1): 113–130.
- McCann K, Holdgate A, Mahammad R & Waddington A (2007) Accuracy of ECG electrode placement by emergency department clinicians. *Emergency Medicine Australasia* 19(5): 442–448.
- Meigas K, Lass J, Kattai R, Karai D & Kaik J (2004) Method of optical self-mixing for pulse wave transit time in comparison with other methods and correlation with blood pressure. In Tuchin VV, Izatt JA, Fujimoto JG (eds) *SPIE Proceedings Vol. 5316: Coherence Domain Optical Methods and Optical Coherence Tomography in Biomedicine VIII*: : 444–453.
- Misciagna S (ed) (2013) *Positron Emission Tomography - Recent Developments in Instrumentation, Research and Clinical Oncological Practice*. InTech. DOI: 10.5772/57537.

- Moukabay T (2007) Willem Einthoven (1860–1927): Father of electrocardiography. *Cardiology Journal* 14(3): 316–317.
- Murgin JM & Arango M (2009) Near-infrared spectroscopy as an index of brain and tissue oxygenation. *British Journal of Anaesthesia* 103 (BJA/PGA Supplement): i3–i13. DOI: 10.1093/bja/aep299.
- Myllylä T, Korhonen V, Surazyński Ł, Zienkiewicz A, Sorvoja H & Myllylä R (2013) Lock-in amplification - a practical technique when utilising high-power LEDs in near-infrared spectroscopy. Symposium Photonics in Measurements (IMEKO), September 16–18, 2013, Gdansk, Poland, Book of abstracts.
- Myllylä T, Sorvoja H, Nikkinen J, Tervonen O, Kiviniemi V & Myllylä R (2011) Instrumentation and method for measuring NIR light absorbed in tissue during MR imaging in medical NIRS measurements, Conference on Novel Biophotonic Techniques and Applications, Munich, Germany, May 22–24, 2011. Sterenberg, HJCM, Vitkin IA (eds) Proceedings of SPIE 8090. Bellingham, Spie-OSA: 1–8.
- Näsi T, Kotilahti K, Noponen T, Nissilä I, Lipiäinen L & Meriläinen P (2010) Correlation of visual-evoked hemodynamic responses and potentials in human brain. *Exp Brain Res* 202:561–570
- Niendorf T, Winter L & Frauenrath T (2012) Electrocardiogram in an MRI Environment: Clinical Needs, Practical Considerations, Safety Implications, Technical Solutions and Future Directions. In Millis R (ed) *Advances in Electrocardiograms - Methods and Analysis*.
- Obrig H, Neufang M, Wenzel R, Kohl M, Steinbrink J, Einhäupl K & Villringer A (2012) Spontaneous Low Frequency Oscillations of Cerebral Hemodynamics and Metabolism in Human Adults. *Neuroimage* 12: 623–639.
- Obrig H (2014) NIRS in clinical neurology — a ‘promising’ tool? *Neuroimage* 85 Part 1(0): 535–546.
- Ogawa S, Lee TM, Kay AR & Tank DW (1990) Brain magnetic resonance imaging with contrast dependent on blood oxygenation. *Proc Nat Acad Sci* 87(24): 9868–9872.
- Ogawa S, Tank DW, Menon R, Ellermann JM, Kim S-G, Merkle H & Ugurbil K (1992) Intrinsic signal changes accompanying sensory stimulation; Functional brain mapping with magnetic resonance imaging. *Proc Natl Acad Sci USA* 89: 5951–5955.
- Okada E, Firbank M, Schweiger M, Arridge SR, Cope M & Delpy DT (1997) Theoretical and experimental investigation of near-infrared light propagation in a model of the adult head. *Appl Opt* 36: 21.
- Peiponen KE, Myllylä R & Priezzhev AV (2009) *Optical Measurement Techniques: Innovations for Industry and the Life Sciences*. Berlin Heidelberg, Springer-Verlag.
- Piper SK, Krueger A, Koch SP, Mehnert J, Habermehl C, Steinbrink J, Obrig H & Schmitz CH (2014) A wearable multi-channel fNIRS system for brain imaging in freely moving subjects. *Neuroimage* 85 Part 1(0): 64–71.
- Popp J, Tuchin VV, Chiou A & Heinemann SH (eds) (2012) *Handbook of Biophotonics*, vol. 2. Wiley.

- Re R, Contini D, Turola M, Spinelli L, Zucchelli L, Caffini M, Cubeddu R & Torricelli A (2013) Multi-channel medical device for time domain functional near infrared spectroscopy based on wavelength space multiplexing. *Biomed Opt Express* 4: 2231–2246.
- Rinck P (2013) *Magnetic Resonance in Medicine. The Basic Textbook of the European Magnetic Resonance Forum*. 7th edition.
- Sandrone S, Bacigaluppi M, Galloni MR, Cappa SF, Moro A, Catani M, Filippi M, Monti MM, Perani D & Martino G (2014) Weighing brain activity with the balance: Angelo Mosso's original manuscripts come to light. *Brain* 137(2): 621–633.
- Sasai S, Homae F, Watanabe H, Sasaki AT, Tanabe HC, Sadato N & Taga G (2012) A NIRS–fMRI study of resting state network. *Neuroimage* 63: 179–193.
- Schelkanova I & Toronov V (2011) Principal and independent component analysis of concomitant functional near infrared spectroscopy and magnetic resonance imaging data. *Proc. SPIE 8088, Diffuse Optical Imaging III, 80881M* (June 14, 2011). DOI: 10.1117/12.889745.
- Scofield JH (1994) A Frequency-Domain Description of a Lock-in Amplifier. *American Journal of Physics* 62(2): 129–133.
- Sharma R (ed) (2012) *Functional Magnetic Resonance Imaging - Advanced Neuroimaging Applications*. InTech. DOI: 10.5772/2512.
- Smith IB (1993) The impact of Stephen Hales on medicine. *Journal of the Royal Society of Medicine* 86(6): 349.
- Sorvoja H (2006) Noninvasive blood pressure pulse detection and blood pressure determination. *Acta Univ. Oul. C* 259.
- Spigulis J (2005) Optical noninvasive monitoring of skin blood pulsations. *Applied Optics* 44(10): 1850–1857. URI: <http://dx.doi.org/10.1364/AO.44.001850>.
- Steinbrink J, Villringer A, Kempf F, Haux D, Boden S & Obrig H (2006) Illuminating the BOLD signal: combined fMRI–fNIRS studies. *Magn Reson Imaging* 24(4): 495–505.
- Strangman G, *et al.* (2002) Non-Invasive Neuroimaging Using Near-Infrared Light. *Biol Psychiatry* 52(7): 697–693.
- Strangman G, Culver JP, Thompson JH & Boas DA (2002) A Quantitative Comparison of Simultaneous BOLD fMRI and NIRS Recordings during Functional Brain Activation. *Neuroimage* 17(2): 719–731.
- Strangman G, Franceschini MA & Boas DA (2003) Factors affecting the accuracy of near-infrared spectroscopy concentration calculations for focal changes in oxygenation parameters. *NeuroImage* 18: 865–879.
- Sugo Y, Sakai T, Terao M, Ukawa T & Ochiai R (2012) The comparison of a novel continuous cardiac output monitor based on pulse wave transit time and echo Doppler during exercise. *Engineering in Medicine and Biology Society (EMBC), 2012 Annual International Conference of the IEEE: 236–239*.
- Tisdall MM, Tachtsidis I, Smith M, Leung TS & Elwell CE (2007) Near-infrared spectroscopic quantification of changes in the concentration of oxidized cytochrome c oxidase in the healthy human brain during hypoxemia. *J Biomed Opt* (2): 024002–7.

- Testud F (2013) Dynamic Magnetic Field Estimation for Magnetic Resonance Imaging. Doktorarbeit, Fakultät für Mathematik und Physik der Albert-Ludwigs-Universität Freiburg im Breisgau Albert-Ludwigs-Universität Freiburg im Breisgau.
- Tong S & Thakor NV (2009) Quantitative EEG analysis methods and clinical applications. Boston, Artech House.
- Tong Y & Frederick Bd (2010) Time lag dependent multimodal processing of concurrent fMRI and near-infrared spectroscopy (NIRS) data suggests a global circulatory origin for low-frequency oscillation signals in human brain. *Neuroimage* 53(2): 553–564.
- Tong Y, Bergethon PR & Frederick Bd (2011) An improved method for mapping cerebrovascular reserve using concurrent fMRI and near-infrared spectroscopy with Regressor Interpolation at Progressive Time Delays (RIPTiDe). *Neuroimage* 56(4): 2047–2057.
- Tong Y & Frederick Bd (2012) Concurrent fNIRS and fMRI processing allows independent visualization of the propagation of pressure waves and bulk blood flow in the cerebral vasculature. *Neuroimage* 61(4): 1419–1427.
- Tong Y, Hocke LM, Licata SC & Frederick Bd (2012) Low-frequency oscillations measured in the periphery with near-infrared spectroscopy are strongly correlated with blood oxygen level-dependent functional magnetic resonance imaging signals. *J Biomed Opt* 17(10): 106004. DOI: 10.1117/1.JBO.17.10.106004.
- Tong Y, Hocke LM, Nickerson LD, Licata SC, Lindsey KP & Frederick Bd (2013) Evaluating the effects of systemic low frequency oscillations measured in the periphery on the independent component analysis results of resting state networks. *Neuroimage* 76(0): 202–215.
- Toronov V, Webb A, Choi JH, Wolf M, Safonova L, Wolf U & Gratton E (2001) Study of local cerebral hemodynamics by frequency-domain near-infrared spectroscopy and correlation with simultaneous acquired functional magnetic resonance imaging. *Optics Express* 9: 417–427.
- Toronov VY, Zhang X & Webb AG (2007) A spatial and temporal comparison of hemodynamic signals measured using optical and functional magnetic resonance imaging during activation in the human primary visual cortex. *Neuroimage* 34(3): 1136–1148.
- Tsuji M, Naruse H, Volpe J & Holtzman D (1995) Reduction of Cytochrome aa3 Measured by Near-Infrared Spectroscopy Predicts Cerebral Energy Loss in Hypoxic Piglets. *Pediatr Res* 37(3): 253–259.
- Tuchin VV (ed) (2002) Handbook of optical biomedical diagnostics. Bellingham, SPIE Press.
- Tuchin VV (2007) Tissue Optics: Light Scattering Methods and Instruments for Medical Diagnosis. Bellingham, SPIE Press. DOI: 10.1117/3.684093.
- Virtanen J (2006) Enhancing the compatibility of surgical robots with magnetic resonance imaging. *Acta Univ Oul C* 241.
- Virtanen J (2011) Monitoring sleep and hypercapnia with near-infrared spectroscopy, Aalto University publication series doctoral dissertations 65/2011.

- Wang T, Zhao H, Wang Z, Hou S & Gao F (2011) Multi-channel Photon Counting DOT System based on Digital Lock-in Detection Technique. *Proc. SPIE 7896, Optical Tomography and Spectroscopy of Tissue IX*. DOI: 10.1117/12.871779.
- Willmann S, Schwarzmaier H, Terenji A, Osterholz J, Meister J & Hering P (2013) Small-volume frequency-domain oximetry: phantom experiments and first in vivo results. *J. Biomed Opt* 8(4): 618–628. DOI: 10.1117/1.1608892.
- Wolf M, Ferrari M & Quaresima V (2007) Progress of near-infrared spectroscopy and topography for brain and muscle clinical applications. *J Biomed Opt* 12(6): 062104. DOI: 10.1117/1.2804899.
- Wyatt JS, Cope M, Delpy DT, Richardson CE, Edwards AD, Wray S & Reynolds EO (1990) Quantitation of cerebral blood volume in human infants by nearinfrared spectroscopy. *J Appl Physiol* 68(3): 1086–1091.
- Xu H, Dehghani H, Pogue BW, Springett R, Swartz HM & Dunn JF (2005) A combination NIR/MRI imaging modality for neurological studies. *Proc Intl Soc Mag Reson Med* 13.
- Ye JC, Tak S, Jang KE, Jung J & Jang J (2009) NIRS-SPM: Statistical parametric mapping for near-infrared spectroscopy. *Neuroimage* 44(2): 428–447.
- Yoon Y, Cho J & Yoon G (2009) Non-constrained Blood Pressure Monitoring Using ECG and PPG for Personal Healthcare. *J Med Syst* 33(4): 261–266.
- Zee P, Arridge SR, Cope M & Delpy DT (1990) The Effect of Optode Positioning on Optical Pathlength in Near Infrared Spectroscopy of Brain. In: Piiper J, Goldstick T & Meyer M (eds) *Oxygen Transport to Tissue XII*. Springer US: 79–84.
- Zee P, Cope M, Arridge SR, Essenpreis M, Potter LA, Edwards AD, Wyatt JS, McCormick DC, Roth SC, Reynolds EOR & Delpy DT (1992) Experimentally measured optical pathlengths for the adult head, calf and forearm and the head of the newborn infant as a function of inter optode spacing. *Advances in Experimental Medicine and Biology* 316: 143–153.

Original papers

- I Myllylä T, Katisko J, Harja J, Sorvoja H & Myllylä R (2007) EMI considerations for wireless data transfer in magnetic resonance imaging (MRI) operating room. The 2nd International Symposium on Medical Information and Communication Technology (ISMICT 07), 11-13 December 2007, Oulu, Finland. Proceedings: 1–4.
- II Sorvoja H, Myllylä T, Kirillin MYu, Sergeeva E, Myllylä R, Elseoud AA, Nikkinen J, Tervonen O & Kiviniemi V (2010) Non-invasive, MRI-compatible fiberoptic device for functional near-IR reflectometry of human brain. *Quantum electronics* 40: 1067–1073.
- III Myllylä T, Elsoud AA, Sorvoja H, Myllylä R, Harja J, Nikkinen J, Tervonen O & Kiviniemi V (2011) Fibre optic sensor for non-invasive monitoring of blood pressure during MRI scanning. *J. Biophoton* 4 (1–2): 98–107.
- IV Myllylä T, Korhonen V, Vihriälä E, Sorvoja H, Hiltunen T, Tervonen O & Kiviniemi V (2012) Human heart pulse wave responses measured simultaneously at several sensor placements by two MR-compatible fibre optic methods. *Journal of Sensors*, vol. 2012, Article ID 769613: 1–8.
- V Myllylä T, Vihriälä E, Korhonen V & Sorvoja H (2013) Case study of ECG signal used as a reference signal in optical pulse transit time measurement of blood flow – The effect of different electrode placements on pulse transit time. *Proc. of SPIE Vol. 8699*: 869903–1–13.
- VI Toronov V, Myllylä T, Kiviniemi V & Tuchin VV (2013) Dynamics of the brain: mathematical models and non-invasive experimental studies. *The European Physical Journal Special Topics* 222(10): 2607–2622.
- VII Myllylä T, Popov A, Korhonen A, Bykov AV & Kinnunen M (2013) Optical sensing of a pulsating liquid in a brain-mimicking phantom. *Proc. of OSA-SPIE 8799*: 87990X–1–7.

Reprinted with permission from University of Oulu (I), Turpion-Moscow Ltd (II), Wiley (III), Hindawi Publishing Corporation (IV), SPIE (V), Springer-Verlag (VI), OSA-SPIE (VII).

Original publications are not included in the electronic version of the dissertation.

480. Ukkonen, Kaisa (2014) Improvement of recombinant protein production in shaken cultures : focus on aeration and enzyme-controlled glucose feeding
481. Peschl, Michael (2014) An architecture for flexible manufacturing systems based on task-driven agents
482. Kangas, Jani (2014) Separation process modelling : highlighting the predictive capabilities of the models and the robustness of the solving strategies
483. Kemppainen, Kalle (2014) Towards simplified deinking systems : a study of the effects of ageing, pre-wetting and alternative pulping strategy on ink behaviour in pulping
484. Mäklin, Jani (2014) Electrical and thermal applications of carbon nanotube films
485. Niemistö, Johanna (2014) Towards sustainable and efficient biofuels production : use of pervaporation in product recovery and purification
486. Liu, Meirong (2014) Efficient super-peer-based coordinated service provision
487. Väyrynen, Eero (2014) Emotion recognition from speech using prosodic features
488. Celentano, Ulrico (2014) Dependable cognitive wireless networking : modelling and design
489. Peräntie, Jani (2014) Electric-field-induced dielectric and caloric effects in relaxor ferroelectrics
490. Aapaoja, Aki (2014) Enhancing value creation of construction projects through early stakeholder involvement and integration
491. Rossi, Pekka M. (2014) Integrated management of groundwater and dependent ecosystems in a Finnish esker
492. Sliz, Rafal (2014) Analysis of wetting and optical properties of materials developed for novel printed solar cells
493. Juntunen, Jouni (2014) Enhancing organizational ambidexterity of the Finnish Defence Forces' supply chain management
494. Hänninen, Kai (2014) Rapid productisation process : managing an unexpected product increment
495. Mehtonen, Saara (2014) The behavior of stabilized high-chromium ferritic stainless steels in hot deformation
496. Majava, Jukka (2014) Product development : drivers, stakeholders, and customer representation during early development

S E R I E S E D I T O R S

A
SCIENTIAE RERUM NATURALIUM

Professor Esa Hohtola

B
HUMANIORA

University Lecturer Santeri Palviainen

C
TECHNICA

Postdoctoral research fellow Sanna Taskila

D
MEDICA

Professor Olli Vuolteenaho

E
SCIENTIAE RERUM SOCIALIUM

University Lecturer Veli-Matti Ulvinen

F
SCRIPTA ACADEMICA

Director Sinikka Eskelinen

G
OECONOMICA

Professor Jari Juga

EDITOR IN CHIEF

Professor Olli Vuolteenaho

PUBLICATIONS EDITOR

Publications Editor Kirsti Nurkkala

ISBN 978-952-62-0506-9 (Paperback)

ISBN 978-952-62-0507-6 (PDF)

ISSN 0355-3213 (Print)

ISSN 1796-2226 (Online)

